CHEMISTRY
A EUROPEAN JOURNAL

DOI: 10.1002/chem.200500930

Cyclic Quaternary Ammonium Ionic Liquids with Perfluoroalkyltrifluoroborates: Synthesis, Characterization, and Properties

Zhi-Bin Zhou,* Hajime Matsumoto,* and Kuniaki Tatsumi[a]

Abstract: New cyclic quaternary ammonium salts, composed of *N*-alkyl-(alkyl ether)-*N*-methylpyrrolidinium, -oxazolidinium, -piperidinium, or -morpholinium cations (alkyl = nC_4H_9, alkyl ether = CH_3OCH_2, $CH_3OCH_2CH_2$) and a perfluoroalkyltrifluoroborate anion ($[R_FBF_3]^-$, $R_F = CF_3$, C_2F_5, nC_3F_7, nC_4F_9), were synthesized and characterized. Most of these salts are liquids at room temperature. The key properties of these salts—phase transitions, thermal stability, density, viscosity, conductivity, and electrochemical windows—were measured and compared to those of their corresponding $[BF_4]^-$ and $[(CF_3SO_2)_2N]^-$ salts. The structural effect on all the above properties was intensively studied in terms of the identity of the cation and anion, variation of the side chain in the cation (i.e., alkyl versus alkyl ether), and change in the length of the perfluoroalkyl group (R_F) in the $[R_FBF_3]^-$ ion. The reduction of Li^+ ions and reoxidation of Li metal took place in pure *N*-butyl-*N*-methylpyrrolidinium pentafluoroethyltrifluoroborate as the supporting electrolyte. Such comprehensive studies enhance the knowledge necessary to design and optimize ionic liquids for many applications, including electrolytes. Some of these new salts show desirable properties, including low melting points, high thermal stabilities, low viscosities, high conductivities, and wide electrochemical windows, and may thus be potential candidates for use as electrolytes in high-energy storage devices. In addition, many salts are ionic plastic crystals.

Keywords: ammonium salts · anions · cations · ionic liquids · perfluoroalkyltrifluoroborates · plastic crystals

Introduction

In recent years, ionic liquids (ILs) have become a rapidly expanding topic of chemical research on account of their unique properties that include a negligible vapor pressure, nonflammability, and good ability to dissolve organic and inorganic compounds, and even polymeric materials.[1] These unusual properties mean that ionic liquids are superior media for a broad range of potential uses, for example, as environmentally friendly solvents for chemical synthesis,[2] biocatalysis,[3] separation technologies,[4] and as solvents or "all-in-one" solvent/templates for nanomaterial preparation.[5] ILs predominantly consist of ionic species and are good ionic conducting materials in the liquid state. Therefore, they are also suitable as solvent-free electrolytes in electrochemical devices and processes,[6] such as rechargeable lithium (Li) batteries,[7,8] electrochemical capacitors,[9] fuel cells,[10] and the electrodeposition of electropositive metals from nuclear fuel at room temperature.[11]

Rechargeable Li batteries are a ubiquitous energy device that is being used worldwide in many types of portable electronic equipment, such as cellular phones, laptop computers, and digital cameras. In the state-of-the-art technologies of 4 V-class rechargeable Li batteries, a mixture of organic aprotic solvents (e.g., ethylene carbonate and diethyl carbonate) and the conducting salt lithium hexafluorophosphate ($LiPF_6$) is generally used as a non-aqueous electrolyte although the safety problem is still an important concern because of the high vapor pressure and low flash point of the organic solvents and the low thermal stability of $LiPF_6$.[12] Driven by the nonvolatility, nonflammability, and good thermal stability of ILs, there is much current interest in the investigation of new electrolyte systems composed of ILs with new stable lithium salts as possible safe replacements for the conventional materials.[6–8,13]

An ionic liquid capable of operating as a supporting electrolyte for 4 V-class rechargeable Li batteries (i.e., Li metal

[a] Dr. Z.-B. Zhou, Dr. H. Matsumoto, Dr. K. Tatsumi
Research Institute for Ubiquitous Energy Devices
National Institute of Advanced Industrial Science and Technology
1-8-31 Midorigaoka, Ikeda, Osaka 563-8577 (Japan)
Fax: (+81) 72-727-9622
E-mail: zb-zhou@vip.tom.com
h-matsumoto@aist.go.jp

Supporting information for this article is available on the WWW under http://www.chemeurj.org/ or from the author.

or carbon as anode material) must have the following properties: 1) a large electrochemical window (i.e., a low cathodic and high anodic potential versus Li^+/Li) that allows the Li^+/Li redox reaction taking place in both the anode and the cathode sides to be reversible; 2) a weakly coordinating nature for its anion to depress ion pairing, which is never absent with the small Li^+ ion in liquid media; 3) low viscosity at room temperature to enhance the mobility of ionic species; and 4) a wide range of operating temperatures (i.e., low melting point and high thermal stability). Recent studies have shown that the highly fluid and conductive 1,3-dialkylimidazolium salts cannot be used as electrolytes for 4 V-class Li batteries, because of the very positive cathodic potential of the 1,3-dialkylimidazolium cations ($\approx$1 V versus Li^+/Li).[7,8a,d] On the other hand, it was revealed that the ILs based on relatively small saturated quaternary ammonium (QA) cations with the electrochemically stable and weakly coordinating anion, bis(trifluoromethanesulfonyl)imide ($[(CF_3SO_2)_2N]^-$, $[TFSI]^-$), offer some promising properties for this purpose.[8] These promising properties mainly include i) wide electrochemical windows on account of the low cathodic potential of the saturated QA cations and the high anodic potential of the $[TFSI]^-$, ii) low viscosities on account of the high flexibility and good charge distribution of the $[TFSI]^-$, and iii) wide stable liquid ranges on account of the low melting point and high thermal stability of the $[TFSI]^-$ salts.[8,13–16] Despite these desirable properties, the inherent high formula weight and large volume of the $[TFSI]^-$ is the evident bottleneck to improve the fluidity and ionic conductivity of its electrolyte—a binary mixture of Li[TFSI] and QA[TFSI]. This is an immediate barrier for the application of the $[TFSI]^-$-based electrolyte to Li batteries, since low conductivity cannot satisfy the requirement of high power. To further optimize the properties of quaternary ammonium ILs for use as an electrolyte in high-energy density devices, there clearly exists an incentive to envision new stable anions with improved features, such as relatively small formula weight and ion size, to circumvent the drawbacks of the $[TFSI]^-$.

Our recent interest in exploring new stable electrolytes for high-energy density devices, such as Li batteries and electrochemical capacitors as reported by Ue and co-workers,[17–19] has led us to introduce a series of weakly coordinating and electrochemically stable fluoro anions, namely perfluoroalkyltrifluoroborate ($[R_FBF_3]^-$, $R_F = CF_3$, C_2F_5, nC_3F_7, nC_4F_9), into the field of ILs.[19–22] In non-aqueous solvent systems, it was shown that one of the lithium salts, $Li[C_2F_5BF_3]$, can offer a comparable performance to the industry standard $LiPF_6$, and a much better performance than $LiBF_4$, for 4 V-class rechargeable Li batteries, indicating that both the cathodic and anodic stabilities of the $[R_FBF_3]^-$ ion are sufficient for its application as an electrolyte in Li batteries.[18] In our research into ILs, we found that the $[R_FBF_3]^-$ ions can form low-melting and low-viscosity ILs with various cations, including imidazolium, aliphatic quaternary ammonium, and alicyclic pyrrolidinium ions.[20–22] This is mainly attributed to a number of favorable features of the $[R_FBF_3]^-$ ion, including low symmetry, good charge distribution, and high conformational degrees of freedom. Another attractive feature for the $[R_FBF_3]^-$ ion is the easy permutation of the perfluoroalkyl (R_F) chain in the $[R_FBF_3]^-$ ion, which not only enables the optimization of a broad range of properties of their ILs, including viscosity and conductivity, but also presents a rich platform to gain significant insight into the influence of the different factors in the anion on the properties of ILs, which were rarely revealed with the common anion in the literature.

As a continuing part of our program aimed at developing low-melting, low-viscosity, and chemically and electrochemically stable ILs as possible safe electrolytes for high-energy density devices,[8,19,21] we conducted a systematic study of the synthesis and characterization of a large number of new cyclic quaternary ammonium (QA) ILs in this study. These ILs are composed of $[R_FBF_3]^-$ ions and four types of saturated cyclic QA cations with a relatively small ion size (total C atoms $\leq$ 10) including *N*-alkyl(alkyl ether)-*N*-methylpyrrolidinium, -oxazolidinium, -piperidinium, and -morpholinium ions. The fundamental properties (e.g., melting point, thermal stability, density, viscosity, ionic conductivity, and electrochemical windows) required for evaluating the applicability of ILs for electrolytes and other applications were determined for all these salts. The corresponding salts with two popular anions, $[BF_4]^-$ and $[TFSI]^-$, were also synthesized and compared. Although the ILs based on these cationic cores with some common anions (e.g., $[TFSI]^-$, $[BF_4]^-$, and $[PF_6]^-$) have been recently reported in several individual studies,[15,22–26] the effect of the different characteristic features of these cations on the properties of their salts is not well understood. This is because there is no unified understanding of how these cyclic ammonium cations affect the properties of their salts. However, this fundamental knowledge is vital for the design and ultimate realization of ILs as "designer solvents" for many applications, including electrolytes for electrochemical devices. In this study, considerable attention is therefore focused toward a comprehensive understanding of the structural effect on the properties of these cyclic QA salts.

Results and Discussion

Synthesis and characterization: The structures of the cations and anions used for preparing the cyclic quaternary ammonium (QA) salts are depicted here; the pyrrolidinium, oxazolidinium, piperidinium, and morpholinium cores are abbreviated as PY, OX, PI, and MO, respectively, and each subscript in the abbreviation denotes the alkyl or alkoxy group in the cation (i.e., CH_3, nC_4H_9, CH_3OCH_2, $CH_3OCH_2CH_2$ groups in the cations are subscripted as 1, 4, 1O1, and 1O2, respectively), consistent with previous usage.[20–22] A total of 52 QA salts were prepared (Table 1).

All 52 salts in Table 1 were synthesized by neutralizing an aqueous solution of quaternary ammonium hydroxide with an equimolar quantity of the acidic solution of the desired

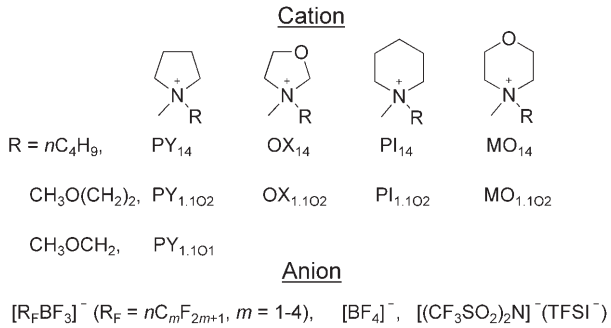

anion, as described in our previous report.[21a] The main advantage of utilizing this acid/base neutralization method is to effectively reduce halide contamination, which is unavoidable in the resultant salts prepared by conventional metathesis reactions (i.e., metathesis of a halide salt of the desired cation with a metal or ammonium salt of the desired anion) in our experience. In the present work, the levels of the residual Br^- and K^+ ions in all the resultant liquid salts prepared by this acid/base reaction, as estimated by X-ray fluorescence spectrometry, were revealed to be less than 20 ppm. The $[R_FBF_3]^-$ ($R_F = CF_3$, C_2F_5, nC_3F_7, nC_4F_9) and $[TFSI]^-$ salts are immiscible with water to some extent owing to the low polarizability and good charge distribution of the highly fluorinated anions that makes the anion–water interactions weak, whereas the $[BF_4]^-$ salts are miscible with water in any ratio as a result of strong anion–water interactions. The water content in the hydrophobic $[R_FBF_3]^-$ and $[TFSI]^-$ salts was <50 ppm after drying under a high vacuum at 70–100 °C for 24 h, and $\approx$100–300 ppm in the hydrophilic $[BF_4]^-$ salts after drying under the same conditions. Therefore, the deviation of the measurement data arising from the presence of halide impurities and water in the resultant ILs is rather limited and should not be a concern in this study.

The structures and compositions of all the 52 salts prepared in Table 1 were confirmed by FAB-MS, elemental analysis, and by ^1H, ^{19}F, and ^{11}B NMR spectroscopy (see the Experimental Section and the Supporting Information). The thermal properties of all the prepared salts were characterized by differential scanning calorimetry (DSC) and thermal gravimetric analysis (TGA). For those salts that are liquid at room temperature, their density (ρ), dynamic viscosity (η), and ionic conductivity (κ) were measured at 25 °C. Electrochemical windows were determined for the salts sharing a common anion, $[C_2F_5BF_3]^-$. All the measurement data are summarized in Tables 1 and 2. The effect of structural variations in the cation and anion on all above properties of their salts will be discussed below based on the results presented in these tables.

Phase behavior, **melting point**, **and glass transition temperature**: The solid–liquid phase transition behavior for each salt in Table 1 was examined by DSC. The data for the glass transition temperature (T_g), crystallization temperature (T_c), solid–solid transition temperature (T_{s-s}), and melting point (T_m), where appropriate, are summarized in Table 1. Figure 1 shows DSC traces for six of the salts (entries 1, 4, 6, 12, 14, and 24) as examples that represent six types of phase transitions observed in all the 52 salts in the present study.

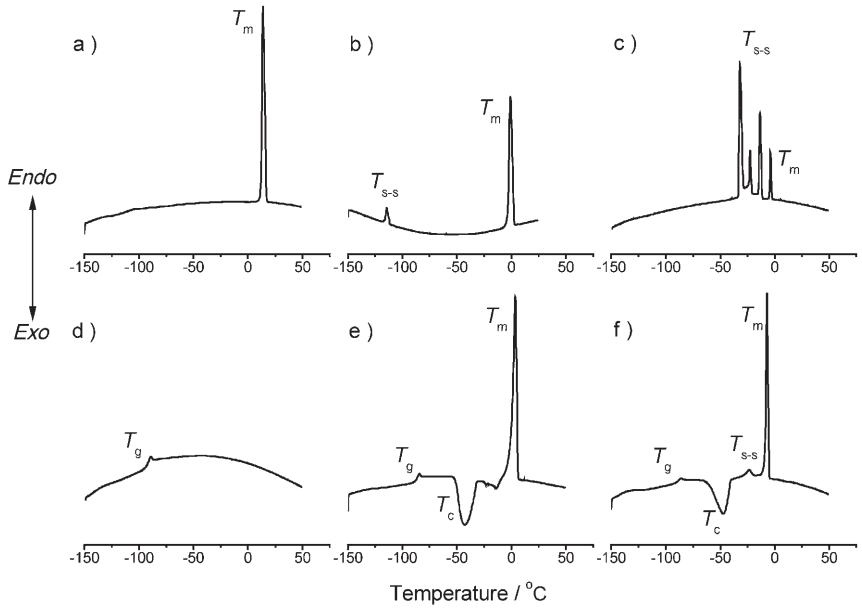

Figure 1. Representative DSC traces recorded at a heating rate of 10 °C in the second cooling/heating cycle. a) $PI_{14}[CF_3BF_3]$: single melting point (T_m); b) $PY_{1.1O2}[C_2F_5BF_3]$: single solid–solid transition (T_{s-s}) before melting (T_m); c) $PY_{1.1O1}[CF_3BF_3]$: multiple solid–solid transitions (T_{s-s}) before melting (T_m); d) $OX_{14}[CF_3BF_3]$: only glass transition (T_g); e) $OX_{1.1O2}[C_2F_5BF_3]$: glass transition (T_g) followed by crystallization (T_c), and melting (T_m); and f) $PI_{1.1O2}[nC_3F_7BF_3]$: glass transition (T_g) followed by crystallization (T_c), solid–solid transition (T_{s-s}), and melting (T_m).

It is worthwhile noting that many cyclic QA salts containing $[R_FBF_3]^-$ displayed single or multiple solid–solid transitions (Figure 1b and c), and finally melted with a melting entropy (ΔS_m) usually $<40\,J\,K^{-1}\,mol^{-1}$ (see Table 1), as observed in the related aliphatic QA salts.[21] As stated in the previous literature,[15,21] the salts exhibiting this remarkable characteristic are ionic plastic crystals, and represent a fascinating class of fast-ion conductors that are attracting considerable attention as all-solid-state electrolytes for high-

Table 1. Physicochemical properties of cyclic quaternary ammonium salts.

Entry	Salts	T_g[a] [°C]	T_c[b] [°C]	T_{s-s}[c] [°C]	T_m[d] [°C]	ΔS_m[e] [J K^{-1} mol^{-1}]	T_d[f] [°C]	ρ[g] [g mL^{-1}]	η[h] [cP]	κ[i] [mS cm^{-1}]
1	$PY_{1.1O1}[CF_3BF_3]$			−33, −24, −14	−4	5.7	227	1.3091	46	7.7
2	$PY_{14}[CF_3BF_3]$				−18	49.4	236	1.2153	137	3.3
3	$PY_{1.1O2}[CF_3BF_3]$				−16	61.9	232	1.2841	87	4.3
4	$OX_{14}[CF_3BF_3]$	−94					238	1.2889	165	2.3
5	$OX_{1.1O2}[CF_3BF_3]$	−86					226	1.3604	134	2.4
6	$PI_{14}[CF_3BF_3]$				12	23.0	244	1.2059	456	1.0
7	$PI_{1.1O2}[CF_3BF_3]$			−46	−16	41.9	234	1.2707	203	1.8
8	$MO_{14}[CF_3BF_3]$	−74					181	1.2728	1035	0.4
9	$MO_{1.1O2}[CF_3BF_3]$			−22, −5	1	26.1	232	1.3477	471	0.7
10	$PY_{1.1O1}[C_2F_5BF_3]$			−51, −16	26	23.7	299	1.3776	37	6.6
11	$PY_{14}[C_2F_5BF_3]$			−93	22	40.4	311	1.2877	71	3.5
12	$PY_{1.1O2}[C_2F_5BF_3]$			−116	−3	53.0	289	1.3490	52	4.5
13	$OX_{14}[C_2F_5BF_3]$				−4	37.0	292	1.3525	108	2.2
14	$OX_{1.1O2}[C_2F_5BF_3]$	−88	−51		1	51.1	293	1.4194	90	2.5
15	$PI_{14}[C_2F_5BF_3]$				41	51.2	308			
16	$PI_{1.1O2}[C_2F_5BF_3]$				−15	80.5	301	1.3349	112	2.2
17	$MO_{14}[C_2F_5BF_3]$	−73					303	1.3404	466	0.5
18	$MO_{1.1O2}[C_2F_5BF_3]$	−78					306	1.4077	260	0.9
19	$PY_{14}[nC_3F_7BF_3]$			−115, −86, −44, 28	53	33.4	327			
20	$PY_{1.1O2}[nC_3F_7BF_3]$			−65	6	60.3	283	1.4059	62	3.3
21	$OX_{14}[nC_3F_7BF_3]$			−99	53	46.1	307			
22	$OX_{1.1O2}[nC_3F_7BF_3]$	−84	−30		10	44.9	293	1.3391	117	1.6
23	$PI_{14}[nC_3F_7BF_3]$				81	50.4	325			
24	$PI_{1.1O2}[nC_3F_7BF_3]$	−92	−62	−29	−9	35.1	297	1.3884	131	1.5
25	$MO_{14}[nC_3F_7BF_3]$			−8	69	35.6	317			
26	$MO_{1.1O2}[nC_3F_7BF_3]$	−75					302	1.4600	777	0.5
27	$PY_{14}[nC_4F_9BF_3]$			−114, −81	61	46.9	324			
28	$PY_{1.1O2}[nC_4F_9BF_3]$	−100	−63		−13	46.3	284	1.4536	84	2.1
29	$OX_{14}[nC_4F_9BF_3]$				54	41.9	275			
30	$OX_{1.1O2}[nC_4F_9BF_3]$	−82	−34		18	56.2	270	1.5125	177	1.0
31	$PI_{14}[nC_4F_9BF_3]$			−91, −84	92	51.8	323			
32	$PI_{1.1O2}[nC_4F_9BF_3]$			−78, −28	20	25.1	298	1.4341	187	0.9
33	$MO_{14}[nC_4F_9BF_3]$			−15, −8, 38	76	32.6	301			
34	$MO_{1.1O2}[nC_4F_9BF_3]$			−12, −1, 36	126	14.9	300			
35	$PY_{1.1O1}[BF_4]$	−114	−61		−18	45.1	290	1.2538	100	6.8
36	$PY_{14}[BF_4]$				150[j]	23.7	403			
37	$PY_{1.1O2}[BF_4]$	−93	−33		12	49.6	390	1.2354	213	2.9
38	$OX_{14}[BF_4]$	−75	−34		−12	11.7	322	1.2387	731	0.8
39	$OX_{1.1O2}[BF_4]$	−70					297	1.3091	704	0.8
40	$PI_{14}[BF_4]$			4, 81	146	22.0	403			
41	$PI_{1.1O2}[BF_4]$	−77					387	1.2162	1240	0.6
42	$MO_{14}[BF_4]$			−54	66	25.6	386			
43	$MO_{1.1O2}[BF_4]$	−58	2		85	56.6	365			
44	$PY_{1.1O1}[TFSI]$			−48	−21	70.7	269	1.4827	40	5.5
45	$PY_{14}[TFSI]$	−89[k]	−54	−30	−19[l]	46.0	431	1.3931[m]	76[n]	2.6[o]
46	$PY_{1.1O2}[TFSI]$	−91					416	1.4539	53	3.7
47	$OX_{14}[TFSI]$	−76	−45		12	43.1	327	1.4645	145	2.1
48	$OX_{1.1O2}[TFSI]$	−73					328[p]	1.5172[q]	117[r]	1.8
49	$PI_{14}[TFSI]$	−77					423	1.3786	182	1.1
50	$PI_{1.1O2}[TFSI]$	−82					417	1.4355	102	2.0
51	$MO_{14}[TFSI]$	−60	−20, 1		35	80.5	398	1.4405	532	0.4
52	$MO_{1.1O2}[TFSI]$	−66					387[s]	1.5055[t]	310[u]	0.6

[a] Glass transition. [b] Crystallization temperature. [c] Solid–solid transition. [d] Melting point. [e] Entropy of fusion ($\Delta S_m = \Delta H_m/T_m$, where ΔH_m is melting enthalpy at T_m[K]). [f] Decomposition temperature. [g] Density at 25 °C. [h] Viscosity at 25 °C. [i] Specific conductivity at 25 °C. [j] Literature value 138 °C.[23] [k] Literature value −87 °C.[15a] [l] Literature value −18 °C.[15a] [m] Literature value 1.41 g mL^{-1}.[15a] [n] Literature value 85 cP.[15a] [o] Literature values 2.2;[15a] 2.6 mS cm^{-1}.[13] [p] Literature value 321 °C.[25b] [q] Literature value 1.53 g mL^{-1}.[25b] [r] Literature value 107 cP.[25b] [s] Literature value 350 °C.[25b] [t] Literature value 1.42 g mL^{-1}.[25b] [u] Literature value 284 cP.[25b]

energy density devices.[27,28] Therefore, the conductivity behavior of these salts and the mixture with their lithium salt will be appreciated in future.

The melting point (T_m) of an organic molecular compound is determined by the strength of its crystal lattice, which is in turn controlled by three main factors: molecular symmetry, intermolecular forces, and conformational degrees of freedom of the molecule.[29] This principle is also applicable to the ILs, as intensively described in a very large number of well-characterized imidazolium and QA

Table 2. Cathodic and anodic limits ($E_{cathodic}$ and E_{anodic} versus ferrocene (Fc)/ferrocenium (Fc^+) at 1.0 mA cm^{-2}) and electrochemical windows (EW) for the $[C_2F_5BF_3]^-$ ionic liquids with various cations determined on a glassy carbon electrode.

Salts	$E_{cathodic}$ [V]	E_{anodic} [V]	EW [V]
EMI[$C_2F_5BF_3$]	−2.50	2.15	4.65
$PY_{1.1O1}$[$C_2F_5BF_3$]	−3.03	2.24	5.27
PY_{14}[$C_2F_5BF_3$]	−3.41	2.24	5.64
$PY_{1.1O2}$[$C_2F_5BF_3$]	−2.99	2.24	5.22
OX_{14}[$C_2F_5BF_3$]	−3.28	2.26	5.54
$OX_{1.1O2}$[$C_2F_5BF_3$]	−2.38	2.27	4.65
PI_{14}[$C_2F_5BF_3$][a]	−3.37	2.15	5.52
$PI_{1.1O2}$[$C_2F_5BF_3$]	−2.85	2.26	5.11
MO_{14}[$C_2F_5BF_3$]	−2.62[b]	2.37	4.99
$MO_{1.1O2}$[$C_2F_5BF_3$]	−2.14	2.34	4.48

[a] Measured at 50 °C. [b] The data was measured at a current density of 0.7 mA cm^{-2}.

salts.[14,15,20,21] Qualitatively, reducing ion symmetry, increasing the ion's conformational degrees of freedom (e.g., utilizing flexible substituents), and improving the charge distribution of the cation and/or anion are effective approaches to reduce the lattice energy of the salts, thus resulting in low-melting salts. Based on these empirical principles and a recent result on the $[C_2F_5BF_3]^-$ salts with pyrrolidinium bearing various lengths of alkyl or alkyl ether side chains,[22] our strategy to prepare low-melting and low-viscosity cyclic QA salts is to incorporate a flexible alkyl or alkyl ether substituent of a medium size, such as *n*-butyl (nC_4H_9), methoxymethyl (CH_3OCH_2), and methoxyethyl ($CH_3OCH_2CH_2$) groups to the cyclic QA cation. An additional advantage for utilizing these three substituents has a beneficial effect on improving the ionic conductivity of their salts because of their relatively small formula weight and size.

Figure 2 shows the melting point (T_m) of the cyclic QA salts in Table 1 that crystallized under the measurement conditions. As shown in Figure 2, low melting points were

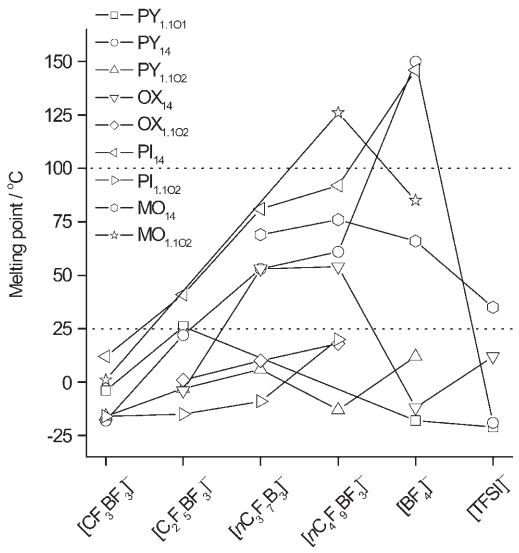

Figure 2. Melting points of various salts.

indeed achieved for most salts in our study. With the three exceptions of $PY_{14}[BF_4]$, $PI_{14}[BF_4]$, and $MO_{1.1O2}[nC_4F_9BF_3]$, all the salts have a melting point of <100 °C, and 38 salts are liquids at room temperature (some of the salts exhibited only a glass transition at an extremely low temperature without melting). Most of the low-melting salts are those containing an alkyl ether side chain (i.e., CH_3OCH_2 or $CH_3OCH_2CH_2$) in the cation, as observed in the aliphatic QA salts.[21,30,31] It can be seen in Figure 2 that, in most cases, the replacement of the *N*-alkyl (nC_4H_9) in the cation with an isoelectronic alkyl ether ($CH_3OCH_2CH_2$) group results in a lowering of the T_m, for example, PY_{14} versus $PY_{1.1O2}$, OX_{14} versus $OX_{1.1O2}$, and PI_{14} versus $PI_{1.1O2}$. Moreover, the PY, OX, and MO cations containing a much longer alkyl ether side chain, such as ethoxyethyl ($CH_3CH_2OCH_2CH_2$), 2-ethoxyethoxyethyl ($CH_3CH_2OCH_2CH_2OCH_2CH_2$), were also found to produce low-melting salts ($T_m<25$ °C or an extremely low T_g without melting),[22,25] while the PY salts containing a longer alkyl side chain in the cation exhibit melting points above room temperature, namely $PY_{15}[C_2F_5BF_3]$ (36 °C), $PY_{16}[C_2F_5BF_3]$ (58 °C), and $PY_{17}[C_2F_5BF_3]$ (52 °C).[22] These results suggest that the utilization of a flexible substituent to increase the conformational degrees of freedom of the cyclic QA cation is an effective approach to lowering the melting points of their salts.

The nature of the anion also significantly affects the melting point of the cyclic QA salts. In the homologous series of the $[R_FBF_3]^-$ ions ($R_F=nC_mF_{2m+1}$, $m=0$–4) salts, the melting points are usually lower for the salts with the smaller $[R_FBF_3]^-$ ($R_F=CF_3$, C_2F_5) than for those with the larger $[R_FBF_3]^-$ ($R_F=nC_3F_7$, nC_4F_9) and high-symmetry $[BF_4]^-$ ions (Figure 2). This suggests that an anion with a low symmetry and a medium size (e.g., $[CF_3BF_3]^-$ and $[C_2F_5BF_3]^-$, in this case reduces the packing efficiency, but without a significant increase of the van der Waals interactions in their salts) favors a lowering of the melting point of its salt, while that with a very large size (e.g., $[nC_3F_7BF_3]^-$ and $[nC_4F_9BF_3]^-$) or high symmetry (e.g., $[BF_4]^-$) tends to increase the melting point owing to the increased van der Waals interactions for the large anions and ordered ion arrangement for the high-symmetry anion. However, all the salts with the large $[TFSI]^-$ ion exhibit low melting points regardless of the cationic species (Figure 2); these results suggest that the high flexibility and low symmetry in the $[TFSI]^-$ ion are dominant over its large size (i.e., van der Waals interactions) in determining the melting point. Generally, the melting point of an ionic liquid is the combined result of many competing interactions that influence the stability of its crystal lattice, and a subtle change in structure has a tremendous impact on its melting point. This is well manifested by the salts with the isomeric cations, as illustrated in Figure 2; for example, for the same $[nC_4F_9BF_3]^-$ ion, $PY_{1.1O2}$ (−13 °C) versus OX_{14} (54 °C), $PI_{1.1O2}$ (−9 °C) versus MO_{14} (76 °C). In the present study, no clear correlations are observed between the structure and chemical composition of these salts and their melting points.

Figure 3 shows the glass transition temperatures (T_g) of the cyclic QA salts that formed glasses under the experimental conditions. It seems that the T_g of these QA salts is mainly determined by the nature of the cation, including ion size and polarity; and the nature of the anion, including ion size, flexibility, and the extent of charge distribution. As can

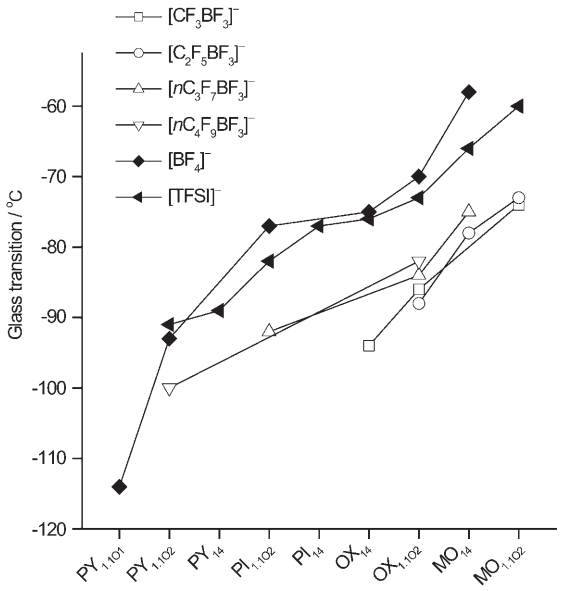

Figure 3. Glass transition temperatures of various salts.

be seen in Figure 3, for a given anion, the T_g values generally increase in the order $PY_{1.1O1} < PY_{1.1O2} < PY_{14} < PI_{1.1O2} < PI_{14} < OX_{14} < OX_{1.1O2} < MO_{14} < MO_{1.1O2}$, indicating both the cationic core and the alkyl (alkyl ether) side chain affect the T_g. In the family of salts containing the alicyclic QA core (i.e., $PY_{1.1O1}$, $PY_{1.1O2}$, PY_{14}, $PI_{1.1O2}$, and PI_{14}), for a common anion, the T_g values increase with increasing size of the cation (the size of the CH_2 unit is larger than that of the oxygen atom), as expected by the increased London dispersion forces. Likewise, in the family of salts containing an ether bond in the cationic core (i.e., OX_{14}, $OX_{1.1O2}$, MO_{14}, and $MO_{1.1O2}$), the T_g values for the salts with the smaller OX cation are lower than those with the larger MO cation (Figure 3). However, one may note that the T_g values are lower for the OX_{14} salts than for their $OX_{1.1O2}$ counterparts, which is opposite to the cation size; the same trend is also observed in the MO_{14} versus $MO_{1.1O2}$ salts (Figure 3). It appears that the polarity of the methoxyethyl ($CH_3OCH_2CH_2$) group in the OX and MO cations predominates over its size and flexibility, thus increasing the dipole–dipole interactions between the ions, which in turn raises the T_g. This effect is more prominent when comparing the T_g of the OX and MO salts with that of the PY and PI salts. The higher T_g for the OX and MO salts suggests the high polarity of their cationic core is the dominant factor in determining the T_g.

For the salts with a common cation, the T_g of the $[R_FBF_3]^-$ salts is much lower than that of the corresponding salts of the $[BF_4]^-$ and $[TFSI]^-$; for example, keeping the $OX_{1.1O2}$ constant, the T_g values increase in the order $[C_2F_5BF_3]^-$, $[CF_3BF_3]^- < [nC_3F_7BF_3]^-$, $[nC_4F_9BF_3]^- \ll [TFSI]^-$, $[BF_4]^-$ (Figure 3), which is quite similar to the trend observed in the aliphatic QA salts of these anions.[21] It seems that the lower T_g for the $[R_FBF_3]^-$ salts is essentially attributable to better charge distribution, more conformational degrees of freedom, and low polarizability residing in the $[R_FBF_3]^-$ ion; these factors which are propitious for weakening the strength of the ion–ion interactions in the salts and hence decrease the T_g, while the higher T_g for the $[TFSI]^-$ salts is probably attributable to its large volume, which is predominant over its high charge distribution and flexibility.

Thermal stability: The short-term thermal stability of all 52 salts in Table 1 was examined by means of TGA experiments. Figure 4 shows the decomposition temperatures (T_d)

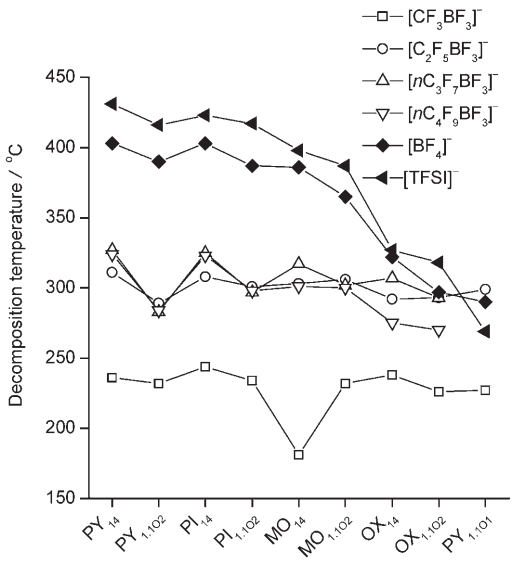

Figure 4. Decomposition temperatures of various salts.

of these salts. It was found that the thermal stability of these salts is significantly affected by the following three factors: 1) the identity of the cationic core, 2) the side chain in the cation, and 3) the identity of the anion. Figure 5 displays the TGA profile for the $[TFSI]^-$ salts with various cations to demonstrate the impact of the variations in the cationic core and side chains of the cation on the thermal stability. The effect of the first two factors on the thermal stability is evident in the series of $[BF_4]^-$ and $[TFSI]^-$ salts. As shown in Table 1 and Figure 5, for the salts sharing a common $[TFSI]^-$ ion, the T_d values decrease in the following order: PY_{14} (431 °C), PI_{14} (423 °C) > $PY_{1.1O2}$ (416 °C), $PI_{1.1O2}$ (417 °C) > MO_{14} (398 °C), $MO_{1.1O2}$ (387 °C) > OX_{14} (327 °C), $OX_{1.1O2}$ (328 °C) > $PY_{1.1O1}$ (269 °C). The same trend was also observed in the series of $[BF_4]^-$ salts (Figure 4). This trend clearly indicates that 1) an ether bond in the cationic core causes a decrease in the thermal stability, which is much more noticeable with the OX cation; 2) replacing the alkyl

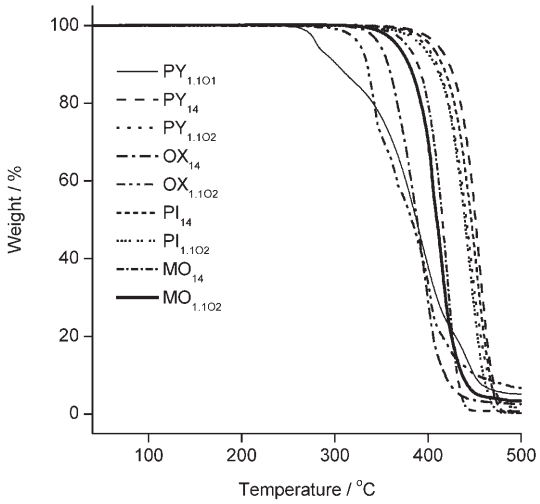

Figure 5. Thermogravimetric analysis traces of the $[(CF_3SO_2)_2N]^-$ ($[TFSI]^-$) salts with various cations.

group (nC_4H_9) in the cation with a methoxyethyl ($CH_3OCH_2CH_2$) group tends to decrease the thermal stability; and 3) a methoxymethyl (CH_3OCH_2) group in the cation results in a remarkable decrease (>100 °C) in the thermal stability. Similar results were also observed in the $[BF_4]^-$ and $[TFSI]^-$ salts with imidazolium cations containing an alkoxymethyl ($ROCH_2$) (T_d<250 °C)[32] versus an alkyl side chain (T_d>400 °C).[33] In addition, the last two effects on the thermal stability are also observable in the $[R_FBF_3]^-$ (R_F= C_2F_5, nC_3F_7, nC_4F_9) salts (Figure 4). These findings suggest that the introduction of ether bonds into the cation, particularly those with an oxygen and a nitrogen atom attached to the same carbon atom (i.e., containing an -NCH_2O- moiety, such as in the OX and $PY_{1.1O1}$ cation), is unsuitable for producing thermally stable ILs. It appears that the low thermal stability of such salts might be partially caused by the relatively high acidity of the protons of the -NCH_2O- moiety.

The identity of the anion also influences the thermal stability of these cyclic QA salts. The T_d values for the $[CF_3BF_3]^-$ salts (181–244 °C) are much lower than those for the $[R_FBF_3]^-$ ($R_F=C_2F_5$, nC_3F_7, nC_4F_9), $[BF_4]^-$, and $[TFSI]^-$ salts (283–431 °C), irrespective of the cationic species (Figure 4 and Table 1). This further reinforces our previous conclusion that the lower thermal stability for the $[CF_3BF_3]^-$ salts is essentially attributed to the thermal lability of the $[CF_3BF_3]^-$ (i.e., $[CF_3BF_3]^- \rightarrow [BF_4]^- + CF_2$ carbene).[20a,21a] In the salts with the $[BF_4]^-$, $[TFSI]^-$, and large $[R_FBF_3]^-$ ($R_F=C_2F_5$, nC_3F_7, nC_4F_9) ions, with the exception of those containing the OX_{14}, $OX_{1.1O2}$ and $PY_{1.1O1}$ cations, for each cation, the T_d values decrease in the order of $[TFSI]^-$ (387–431 °C) > $[BF_4]^-$ (365–403 °C) ≫ $[R_FBF_3]^-$ (283–327 °C). This trend in T_d is consistent with that observed in the related imidazolium and aliphatic QA salts.[20a,21a] The lower thermal stability for the $[R_FBF_3]^-$ salts can be ascribed to the pyrolysis of the $[R_FBF_3]^-$ ions at relatively low temperatures. However, such a difference in the thermal stability significantly diminished in the corresponding salts with the OX_{14}, $OX_{1.1O2}$, and $PY_{1.1O1}$ cations (Figure 4). This may be explained by the thermal lability of these three cations, as previously discussed with respect to the influence of the cationic species on the thermal stability.

Density: The density of the 38 room-temperature liquid salts was measured at 25 °C (Table 1). Figure 6 shows the density (ρ) of these liquid salts. The values for the density vary between 1.21 and 1.52 g mL^{-1}. For a given anion, the density gradually decreases in the order $OX_{1.1O2} > MO_{1.1O2} > PY_{1.1O1} > OX_{14} > PY_{1.1O2} > MO_{14} > PI_{1.1O2} > PY_{14} > PI_{14}$. From this trend, it is apparent that the density is increased by 1) reducing the size of the cationic core (e.g., MO versus OX, PI versus PY), and 2) having an ether bond in the cationic core (e.g., OX versus PY, and MO versus PI) and/or in the side-chain group of the cation (e.g., $OX_{1.1O2}$ versus OX_{14}, $PY_{1.1O2}$ versus PY_{14}, $PI_{1.1O2}$ versus PI_{14}). The observed increase in density caused by replacing the CH_2 unit with an oxygen atom in the cation (i.e., incorporating an ether bond to the cationic core or side chain) should be attributed to the relatively smaller van der Waals volume and higher mass for the oxygen atom than for the CH_2 unit. In addition, for the salts with the isomeric cations, the density is slightly higher for the salts containing an ether bond in the cationic core than for those containing an ether bond in the side chain; for example, OX_{14} versus $PY_{1.1O2}$, and MO_{14} versus $PI_{1.1O2}$ (Figure 6).

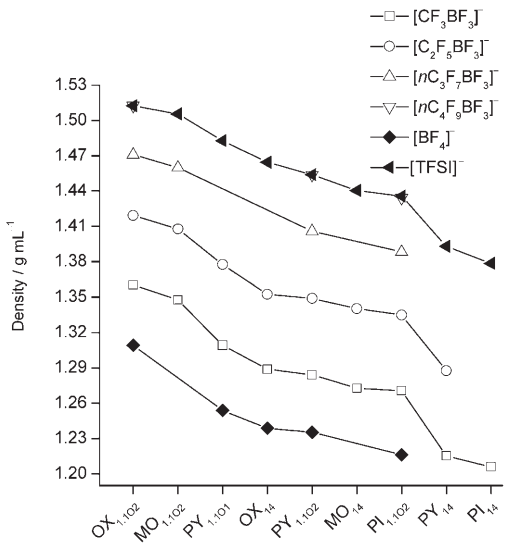

Figure 6. Density of various liquid salts at 25 °C.

For the salts with a common cation, the density increases regularly with increasing bulkiness of the fluoro anions in the order $[BF_4]^- < [CF_3BF_3]^- < [C_2F_5BF_3]^- < [nC_3F_7BF_3]^- < [nC_4F_9BF_3]^- \approx [TFSI]^-$ (Figure 6), as expected by the large mass and small van der Waals radii of the fluorine atom. In the homologous series of the $[R_FBF_3]^-$ ($R_F=nC_mF_{2m+1}$, m= 0–4) salts, for a common cation, the addition of a CF_2 unit

to the perfluoroalkyl (R_F) chain in the anion linearly increases the density by $\approx 0.07\ g\,mL^{-1}$.

Viscosity: Viscosity is a decisive parameter for assessing ILs with respect to their use as media in chemical and electrochemical applications, because of its strong impact on the rate of mass transport. The electrolytes in many electrochemical devices are required to operate in ambient temperature ranges, so the ILs used as supporting electrolytes should have low viscosities at room temperature. Currently, one of the largest barriers for the application of the pure QA liquid salts to electrolytes is their high viscosity at room temperature. Therefore, the fundamental understanding of the factors that essentially control the viscosity of the cyclic QA liquids is of vital importance for the design of new QA liquids with high fluidity at room temperature.

Figure 7 shows the dynamic viscosity (η) of the 38 room-temperature liquid salts at 25 °C (Table 1). The viscosity values fall in the wide range of 37–1240 cP. It seems that the

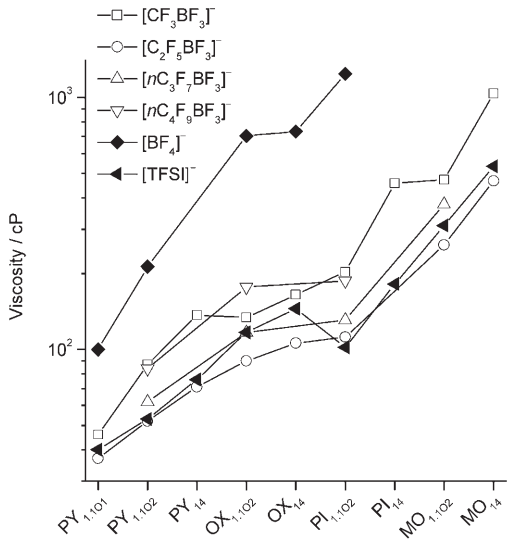

Figure 7. Viscosity of various liquid salts at 25 °C.

viscosity of these cyclic ILs is largely governed by van der Waals interactions, the degree of freedom within the ion, ion shape, and Coulombic forces (mainly in the case of the salts composed of small ions), while hydrogen-bonding interactions are less significant on account of the very weak basicity of the fluoro anions used in this study. The van der Waals interactions in these ILs are mainly contributed from London dispersion forces, determined by the ion size, and dipole–dipole attractions, determined by the polarity of the ion.

As shown in Figure 7, for the salts sharing a common anion, with the exception of $PI_{1.1O2}$[TFSI], the viscosity generally increases in the order $PY_{1.1O1} < PY_{1.1O2} < PY_{14} < OX_{1.1O2} < OX_{14} < PI_{1.1O2} < PI_{14} < MO_{1.1O2} < MO_{14}$. From this trend, it is evident that the viscosity is lower for the salts containing a five-membered cationic core (i.e., PY and OX) than for those containing a six-membered cationic core (i.e., PI and MO), suggesting that the overall cation-dependent trend in the viscosity is essentially under the control of van der Waals interactions.

For the salts with the same cationic core and a common anion, the introduction of an ether bond to the side-chain group of the cation (i.e., replacing the nC_4H_9 group with a $CH_3OCH_2CH_2$ group) uniformly reduces the viscosity (Figure 7); for example, $PY_{1.1O2}$ versus PY_{14}, $OX_{1.1O2}$ versus OX_{14}, $PI_{1.1O2}$ versus PI_{14}, $MO_{1.1O2}$ versus MO_{14}, as observed in the aliphatic QA salts.[21] This effect is more remarkable for the salts containing a much longer alkyl ether side chain, for example, $PY_{1.1O2O2}[C_2F_5BF_3]$ (54 cP), $PY_{1.2O2}[C_2F_5BF_3]$ (49 cP) versus $PY_{14}[C_2F_5BF_3]$ (71 cP) at 25 °C.[22] Generally, the alkyl ether side chain (e.g., $CH_3OCH_2CH_2$) is more flexible, but more polar than the alkyl chain (e.g., nC_4H_9), the flexibility is beneficial to lowering the viscosity by virtue of the increase of conformational degrees of freedom, while the polarity tends to increase the viscosity on account of the increase of dipole–dipole attractions. The above trend in viscosity suggests that the flexibility of the alkyl ether side chain predominates over its polarity, thus reducing the viscosity. In contrast, the incorporation of an ether bond into the alicyclic cationic core (i.e., replacing a CH_2 unit in the PY and PI cores with an oxygen atom) causes a significant increase in the viscosity (Figure 7); for example, $PY_{1.1O2}$, PY_{14} versus $OX_{1.1O2}$, OX_{14}, and $PI_{1.1O2}$, PI_{14} versus $MO_{1.1O2}$, MO_{14}. This effect is well displayed by the large difference in viscosity of the two salts with the isomeric cations; for example, keeping the $[CF_3BF_3]^-$ constant, $PY_{1.1O2}$ (87 cP) versus OX_{14} (165 cP), $PI_{1.1O2}$ (203 cP) versus MO_{14} (1035 cP). As a general trend, changing the oxygen atom from the side chain to the cationic core increases the viscosity by 2–3 times for the salts containing the five-membered ring cation (i.e., OX_{14} versus $PY_{1.1O2}$, Table 1), and by ≈ 5 times for the salts containing the six-membered ring cation (i.e., MO_{14} versus $PI_{1.1O2}$, Table 1). These examples impressively indicate how a slight change in the cation dramatically changes the viscosity, which is rarely observed in the reported literature. Since having an ether bond in the alicyclic cationic core results in an increase in the polarity of the cation, but not in an increase in its conformation degrees of freedom owing to the rigidity of the cationic core, it seems reasonable that the polarity of the OX and MO cations is the predominant factor to account for the high viscosity of their salts.

A comparison of the viscosity of the alicyclic PY salts with that of the aliphatic QA ones clearly displays the impact of the ion shape. Although the PY core has a high rigidity, for a fixed anion, the viscosities of the PY salts are all lower than those of the aliphatic QA salts with a comparable cation (i.e., containing the same number of carbons in the cation), and even lower than the salts with a smaller aliphatic QA cation, for example, $PY_{14}[CF_3BF_3]$ (137 cP) < $N_{1224}[CF_3BF_3]$ (210 cP) (nine carbon atoms in each cation), $PY_{1.1O2}[CF_3BF_3]$ (87 cP, eight carbon atoms) < $N_{112.1O2}$-$[CF_3BF_3]$ (97 cP, seven carbon atoms)[21] < $N_{122.1O2}[CF_3BF_3]$

(108 cP, eight carbon atoms).[21] This result evidently indicates that the quasi-flat shape of the PY core, as illustrated by its crystal structure,[34] plays a dominant role in lowering the viscosity. However, such an effect is not observed in the salts with the six-membered PI cation, which should be attributed to the chair conformation and high rigidity of the PI core. All the above results clearly indicate that 1) among the four types of cyclic QA cations used in this study, the PY cation is the best one for producing low-viscosity ILs, and 2) having an ether bond in the side chain of the QA cation favors an enhancement of the fluidity of the QA salts, while that in the cationic core results in a high viscosity.

In salts with a common cation, the viscosity generally increases in the anion order of $[C_2F_5BF_3]^- \approx [TFSI]^- < [nC_3F_7BF_3]^- < [CF_3BF_3]^-$, $[nC_4F_9BF_3]^- << [BF_4]^-$ (Figure 7), in good agreement with the trend observed in the aliphatic QA salts with these anions.[21a] This trend in viscosity can be interpreted in terms of the competing influence of the following three factors: van der Waals interactions, Coulombic forces, and conformational degrees of freedom in the anion. The highest viscosity for the $[BF_4]^-$ ILs is essentially attributed to the lack of conformational degrees of freedom within the rigid $[BF_4]^-$ ion, and the relatively strong Coulombic forces owing to the smallest size of the $[BF_4]^-$ ion among the anions in the present study. The much lower viscosity for the $[R_FBF_3]^-$ ($R_F = CF_3$, C_2F_5, nC_3F_7, nC_4F_9) salts than for their $[BF_4]^-$ counterparts can be explained by the more conformational degrees of freedom in the $[R_FBF_3]^-$ versus $[BF_4]^-$ ions and the decreased Coulombic forces from the improved charge distribution and increased size of the $[R_FBF_3]^-$ versus $[BF_4]^-$ ions. Furthermore, it can be inferred that the influence on the viscosity of the increase in conformational degrees of freedom and the decrease in Coulombic forces prevail over the increase in van der Waals interactions caused by the increased the anion size ($[R_FBF_3]^-$ versus $[BF_4]^-$). However, the viscosity is dramatically higher for the salts with the smaller $[CF_3BF_3]^-$ ion than for those with the larger $[R_FBF_3]^-$ ion ($R_F = C_2F_5$, nC_3F_7), which is opposite to the trend found for the anion size. It seems that the higher viscosity for the $[CF_3BF_3]^-$ salts may be attributable to the lower conformational degrees of freedom and the stronger Coulombic forces in the $[CF_3BF_3]^-$ salts owing to the smaller size of the $[CF_3BF_3]^-$ ion, as in the case of the $[BF_4]^-$ salts. In the series of $[R_FBF_3]^-$ ($R_F = C_2F_5$, nC_3F_7, nC_4F_9) salts, the viscosity increases with increasing length of the perfluoroalkyl (R_F) chain in the $[R_FBF_3]^-$. This suggests that the van der Waals interactions have taken over the conformational degrees of freedom and the Coulombic forces to govern the viscosity. Among the homologous series of $[nC_mF_{2m+1}BF_3]^-$ ($m = 0$–4) salts with a common cation, the $[C_2F_5BF_3]^-$ salts exhibit the lowest viscosities (37–466 cP at 25 °C) in all cases on account of a relatively high number of conformational degrees of freedom in conjunction with a medium size for the $[C_2F_5BF_3]^-$. The viscosity of the $[TFSI]^-$ salts (40–532 cP at 25 °C) is comparable to that of the corresponding $[C_2F_5BF_3]^-$ salts (Figure 7), although the size of the $[TFSI]^-$ ion is much larger than that of $[C_2F_5BF_3]^-$. This may be attributable to the more flexible nature of the $[TFSI]^-$ ion, which predominates over its large size to determine the viscosity. From these findings, it could be anticipated that the inorganic, weakly coordinating fluoro anions, such as $[PF_6]^-$ and $[AsF_6]^-$, form high-viscosity ILs with the cations used in the present study, because of the lack of conformational degrees of freedom in these anions, as in the case of $[BF_4]^-$. This is also true for the salts with the large, rigid, and weakly coordinating orthoborate anions (e.g., bis(oxalato)borate $[BOB]^-$), as already indicated by the extremely high viscosities for their salts.[31b] On the base of the above understanding of the factors in the anion that affect the viscosity of ILs, we can conclude that, in the search of low-viscosity ILs, the investigator should pay more attention to the anion with some conformational degrees of freedom and a medium size rather than weakly coordinating ability.

Finally, it is worth mentioning that both the cation- and anion-dependent trends of viscosity at 25 °C are not exactly consistent with those for T_g (see Figures 3 and 7), although it was reported that the T_g of ILs is a fairly good measure of the ion mobility: the lower the T_g, the weaker are the cohesive forces in the salts, hence the more fluid the ILs are in many cases.[14b,31] This result clearly indicates that the T_g of ILs is not the only factor governing the viscosity. Angell and co-workers recently reported that the fragility of the ILs (the rate at which the transport properties change with temperature near the glass transition) is another important factor determining the fluid behavior of ILs in ambient temperature range.[31a] The difference in fragility may exist in our salts given the diversity of their structure, and this might be a valid interpretation of the observed discrepancy between the trend of the viscosity at room temperature (25 °C) and glass transitions in the present study.

Conductivity: The conductivity of an ionic liquid is of vital importance if it is to be considered as a supporting electrolyte in electrochemical devices. It has been reported that the ionic conductivity of ILs is mainly governed by their viscosity, formula weight, density, and ion size.[33a] This is also true for the salts in the present study. Figure 8 shows the specific conductivity (κ) of the 38 room-temperature liquid salts at 25 °C (Table 1). The conductivity values of these salts cover the range of 0.4–7.7 mS cm^{-1}. For the salts with a common anion, the conductivity generally decreased in the order $PY_{1.1O1} > PY_{1.1O2} > PY_{14} > OX_{1.1O2} > OX_{14}$, $PI_{1.1O2} > PI_{14} > MO_{1.1O2} > MO_{14}$. This cation trend is expected by the increased viscosity (compare Figure 7 with Figure 8; for a given anion, the trend in viscosity is exactly opposite to that of the conductivity), formula weight, and cation size. It is clear from this trend that the PY cation is the best one to produce highly conductive ILs within the scope of the cyclic QA cations investigated in this study. Notably, for a given anion, the conductivity for the PY salts is evidently higher than that for the aliphatic QA salts with a comparable cation, and even higher than that for salts with a smaller ali-

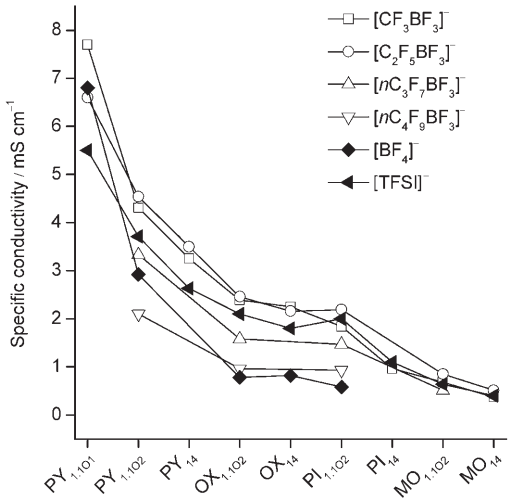

Figure 8. Specific conductivity of various liquid salts at 25 °C.

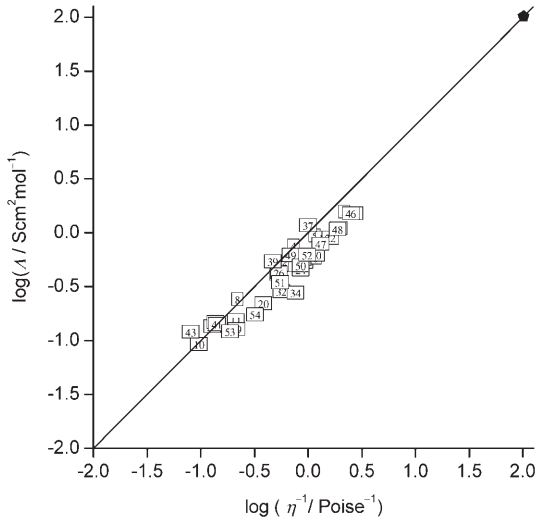

Figure 9. Equivalent conductivity (Λ) versus reciprocal viscosity (η^{-1}) at 25 °C in a common logarithm form for the 38 room-temperature liquid salts given in Table 1 (the numbering is consistent with the entry numbers in Table 1). The solid line is the "ideal" Walden product line fixed with 1 mol L^{-1} aqueous KCl solutions.[31]

phatic QA cation, for example, $PY_{1.1O2}[C_2F_5BF_3]$ (4.5 mS cm^{-1}) > $N_{112.1O2}[C_2F_5BF_3]$ (3.8 mS cm^{-1})[21a] > $N_{122.1O2}$-$[C_2F_5BF_3]$ (3.2 mS cm^{-1}).[21a] This can be explained by the lower viscosities for the PY salts (vide supra).

For salts with a common cation, with the exception of the smallest, $PY_{1.1O1}$, the conductivity generally decreases in the order $[C_2F_5BF_3]^-$, $[CF_3BF_3]^- > [TFSI]^- > [nC_3F_7BF_3]^- > [BF_4]^-$, $[nC_4F_9BF_3]^-$. This anion trend is similar to that observed in the corresponding imidazolium and aliphatic QA salts with these anions,[20a,21a] and is the combined result of several competing factors that affect the conductivity, including the viscosity, formula weight, and ion size, as explained in previous reports.[20a,21a] The difference in conductivity becomes smaller with increasing viscosity (see Figures 8 and 7), and is not noticeable in the most viscous salts containing the MO cation with various anions (Figure 8). This suggests that the transport of ions in these highly viscous salts is more dependent on the fluidity. The $[C_2F_5BF_3]^-$ salts generally show a higher conductivity than the corresponding salts of the $[TFSI]^-$, although they have comparable viscosities, which clearly indicates that an anion with a low formula weight and small size is favorable for the production of highly conductive ILs. Among the 38 room-temperature liquid salts in Table 1, the salts with the smallest cation, $PY_{1.1O1}$, show the highest conductivities, for example, $PY_{1.1O1}[CF_3BF_3]$ (7.7 mScm^{-1}), $PY_{1.1O1}[BF_4]$ (6.8 mScm^{-1}), and $PY_{1.1O1}[C_2F_5BF_3]$ (6.6 mScm^{-1}), mainly owing to their lowest viscosities and the lowest formula weight of the $PY_{1.1O1}$.

It was noted that the empirical Walden rule for dilute electrolyte solutions is applicable to pure ILs, although the exact reason for its applicability in ILs is not yet well understood.[31] Figure 9 shows the equivalent conductivity (Λ) versus the reciprocal viscosity (η^{-1}) in logarithmic form for the 38 room-temperature liquid salts at 25 °C (Table 1), in which $\Lambda = \kappa M/\rho$, M is the formula weight, κ is the specific conductivity, and ρ is the density of the respective salts. It seems that the Walden rule may be valid for the salts in the present study because a plot of $\log\Lambda$ versus $\log\eta^{-1}$ at 25 °C for all these liquid salts (Figure 9) lies on or around the so-called "ideal" Walden product line determined with 1 mol L^{-1} aqueous KCl solutions, as described by Angell and co-workers.[31]

Electrochemical stability: One of the reasons for the recent growing interest in the QA salts is the low cathodic potentials of the QA cations compared to 1,3-dialkylimidazolium cations, hence the wide electrochemical windows for their salts, which may allow them to be used as solvent-free supporting electrolytes in high-energy density devices, including Li batteries and electrochemical capacitors, to improve their safety.[8,9b] Therefore, of particular interest is the relationship between the cationic and anionic structures of the ILs and their electrochemical windows. In previous studies, we revealed that the cathodic limit of the QA salts with the anions used in this study is determined by the reduction of the respective QA cations, while their anodic limit is governed by the oxidation of the respective anions;[21a] however, in the case of the 1,3-dialkylimidazolium salts, both the cathodic and the anodic decomposition are limited by the 1,3-dialkylimidazolium cations.[19,20a] To compare the relative cathodic stability of the cyclic QA cations in the present study, the QA salts with a common anion, $[C_2F_5BF_3]^-$, were investigated by linear-sweep voltammetry on a glassy carbon electrode at 25 °C, except for the salt $PI_{14}[C_2F_5BF_3]$ (T_m = 41 °C), which was measured at 50 °C. Figure 10 shows the linear-sweep voltammograms of the nine cyclic QA salts with $[C_2F_5BF_3]^-$, and of $EMI[C_2F_5BF_3]$ (EMI = 1-ethyl-3-methylimidazolium) for comparison. The potentials for all the salts are given versus the ferrocene (Fc)/ferrocenium

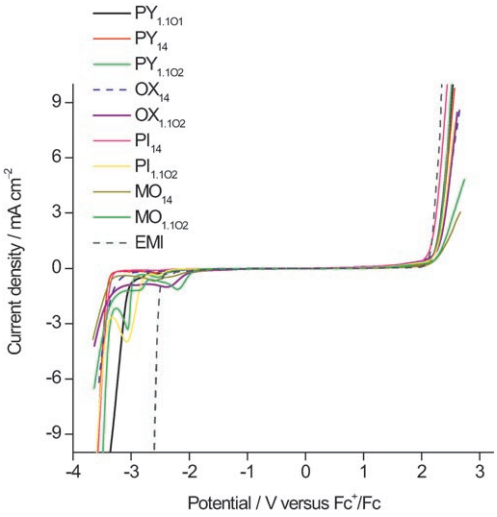

Figure 10. Linear-sweep voltammograms of various ionic liquids obtained on a glassy carbon working electrode (surface area: 7.85×10^{-3} cm^2) in the first scan; scan rate: 50 mV s^{-1}; measurement temperature: 25 °C; counterelectrode: a platinum (Pt) wire; potentials (V) were referenced to ferrocene (Fc)/ferrocenium (Fc^+) redox couple in each salt; the data for EMI[$C_2F_5BF_3$] (EMI = 1-ethyl-3-methylimidazolium) were from the literature.[20a]

(Fc^+) redox couple as the internal standard, because the potential of the Fc/Fc^+ couple is little affected by non-aqueous solvents.[35] The measurement data for the cathodic ($E_{cathodic}$) and anodic (E_{anodic}) limits, and electrochemical windows ($EW = E_{anodic} - E_{cathodic}$) of these salts are summarized in Table 2, in which the values for the respective $E_{cathodic}$ and E_{anodic} are defined as the potential at which the current density reached 1.0 mA cm^{-2}.

As shown in Figure 10, the cathodic stability of these QA salts is significantly affected by the cationic species, and increases in the order of $OX_{1.1O2}$, $MO_{1.1O2} < EMI < MO_{14}$, $PI_{1.1O2}$, $PY_{1.1O2}$, $PY_{1.1O1} < OX_{14} < PI_{14}$, PY_{14}, as indicated by the values of their cathodic limit potential (Table 2). It is apparent from this order that 1) the cyclic QA cations without ether bonds in their built-in structure (i.e., PI_{14} and PY_{14}) show the strongest resistance toward reduction, and 2) having an ether bond in either the side chain or the cationic core of the QA cation generally results in a decrease in the cathodic stability to a lesser or greater extent, which may be ascribed to the reduction of the ether bond of the QA cation at a more positive potential relative to that of the positively charged nitrogen atom of the QA, as is the case for the related aliphatic QA salts.[21a] Notably, the effect of the ether bond on the cathodic stability is much more significant for the QA salts containing two ether bonds in the cations (i.e., $OX_{1.1O2}$ and $MO_{1.1O2}$), as indicated by the most positive cathodic limits for the $OX_{1.1O2}$ (2.38 V) and $MO_{1.1O2}$ (2.14 V) cations, which are even more positive than the EMI cation (2.50 V) (Table 2). This result clearly indicates that not all saturated QA cations are more resistant toward reduction than 1,3-dialkylimidazolium cations. Furthermore, it can be anticipated that the QA salts of the other anions in the present study also show a similar trend in cathodic stability, as shown in Figure 10, because their cathodic limits are little affected by these anions.[21a,22a]

With regard to the anodic stability, as seen in Figure 10, all these cyclic QA salts with $[C_2F_5BF_3]^-$ show nearly equivalent anodic stability at 25 °C, as indicated by the close values of their anodic limit potential (Table 2). The exception is $PI_{14}[C_2F_5BF_3]$, which was measured at a higher temperature of 50 °C; it exhibited a slightly lower anodic limit, as expected from the Nernst equation. All these cyclic QA salts are more stable against oxidation than EMI[$C_2F_5BF_3$] (Figure 10). This is supported by our previous results, which showed that the anodic decomposition of the QA salts are governed by the oxidation of their anionic species while that of the 1,3-dialkylimidazolium salts with electrochemical stable anions are limited by 1,3-dialkylimidazolium cations.[20a,21a] In other words, the $[R_FBF_3]^-$ ($R_F = nC_mF_{2m+1}$, $m = 0$–4) and $[TFSI]^-$ ions are more resistant toward oxidation than 1,3-dialkylimidazolium cations.

Our key objective is to find highly fluid, conductive, and electrochemically stable ILs as supporting electrolytes for 4 V-class Li batteries. Therefore, electrodeposition investigations of the very electropositive Li metal from pure QA-$[R_FBF_3]$ salts are of fundamental importance. To date, among the liquid salts investigated, the electrodeposition of Li metal in pure room-temperature ILs (without addition of any additives) was obtained only in the QA salts with $[TFSI]^-$.[8a,d,13] In the present study, the $PY_{14}[C_2F_5BF_3]$ salt was chosen as an example for this purpose because of its very negative cathodic limit (−3.41 V versus Fc/Fc^+) and low viscosity (71 cP at 25 °C). Taking into account the fact that the redox potential of Li is ≈−3.2 V versus Fc/Fc^+ in propylene carbonate and liquid QA[TFSI] salts,[8d] it seems possible that the electrodeposition of Li metal in pure PY_{14}-$[C_2F_5BF_3]$ could be realized. Figure 11 shows the cyclic vol-

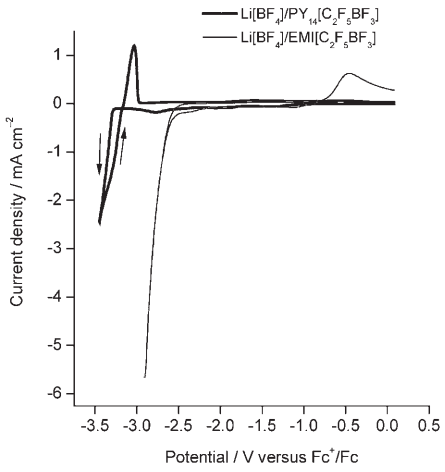

Figure 11. Cyclic voltammograms of a) *N*-butyl-*N*-methylpyrrolidinium pentafluoroethyltrifluoroborate ($PY_{14}[C_2F_5BF_3]$), and b) EMI[$C_2F_5BF_3$] (EMI = 1-ethyl-3-methylimidazolium) containing 0.3 mol kg^{-1} of Li[BF_4] obtained on an Ni electrode (surface area: 1.77×10^{-3} cm^2); scan rate: 50 mV s^{-1}; measurement temperature: 25 °C.

tammograms of 0.3 mol kg^{-1} of $LiBF_4$ in pure $PY_{14}[C_2F_5BF_3]$ and $EMI[C_2F_5BF_3]$, respectively, on an Ni electrode (Ni was used to avoid lithium alloy formation).[35] Indeed, a pair of peaks characteristic of the reduction of Li^+ ions and reoxidation of Li metal were observed at ≈ -3.2 V with $PY_{14}[C_2F_5BF_3]$, which is in excellent agreement with the redox potential of Li in the QA[TFSI].[8d] This preliminary result suggests that 1) both the PY_{14} cation and $[C_2F_5BF_3]^-$ have sufficient cathodic stability to allow the electrodeposition of Li metal, and 2) those of the liquid QA salts with $[R_FBF_3]^-$ ions having a low reduction potential, such as $PY_{14}[C_2F_5BF_3]$, may be potential candidates for the use of supporting electrolytes for 4 V-class Li batteries. However, no electroreduction of Li^+ ions, except for irreversible reduction of the EMI cations, was observed in pure $EMI[C_2F_5BF_3]$ as the supporting electrolyte (Figure 11), which should be attributed to the fact that the cathodic limit of $EMI[C_2F_5BF_3]$ (-2.50 V versus Fc/Fc^+) is more positive than the redox potential of Li (-3.2 V versus Fc/Fc^+).

Conclusion

New cyclic quaternary ammonium salts comprising *N*-alkyl-(alkyl ether)-*N*-methylpyrrolidinium, -oxazolidinium, -piperidinium, and -morpholinium (alkyl = nC_4H_9, alkyl ether = CH_3OCH_2, $CH_3OCH_2CH_2$) with $[R_FBF_3]^-$ ($R_F = CF_3$, C_2F_5, nC_3F_7, nC_4F_9) were synthesized and characterized. Most of them are liquids at room temperature. Their key properties—phase transitions, thermal stability, density, viscosity, specific conductivity, and electrochemical windows, which are necessary for evaluating the applicability of ILs for the use of electrolytes in electrochemical devices—were determined and were compared to those of the corresponding $[BF_4]^-$ and $[(CF_3SO_2)_2N]^-$ salts. It was found that all above properties were significantly affected by the identity of the cation (namely, pyrrolidinium, oxazolidinium, piperidinium, and morpholinium) and anion (namely, $[R_FBF_3]^-$, $[BF_4]^-$, and $[(CF_3SO_2)_2N]^-$), the variation of the side chain in the cation (i.e., alkyl versus alkyl ether), and the change in the length of the perfluoroalkyl group (R_F) in the $[R_FBF_3]^-$. These systematic studies not only improved the basic understanding of the structural effect on the properties of ionic liquids, but they also enriched the fundamental knowledge base of ionic liquids, which is beneficial to the design and optimization of ionic liquids as "designer solvents" for many applications.

Salts with pyrrolidinium and piperidinium cations generally display lower viscosities and higher conductivities than those with the respective oxazolidinium and morpholinium cations. The presence of an ether bond in the side chain of the cation favors an increase in the fluidity and conductivity; however, it causes a remarkable decrease in the thermal and electrochemical (in the cathodic direction) stability of their salts. Liquid salts with $[R_FBF_3]^-$ show much lower viscosities than the corresponding salt with $[BF_4]^-$, owing to a better charge distribution and more conformational degrees of freedom for the $[R_FBF_3]^-$. The $[C_2F_5BF_3]^-$ salts have the lowest viscosities and are comparable to those of their $[(CF_3SO_2)_2N]^-$ analogues. The reduction of Li^+ ions and reoxidation of Li metal was observed in pure *N*-butyl-*N*-methylpyrrolidinium pentafluoroethyltrifluoroborate ($PY_{14}[C_2F_5BF_3]$). Based on the characterization and understanding of the cyclic QA liquid salts, we may conclude that, among the new $[R_FBF_3]^-$ ionic liquids, those having a low melting point, low viscosities, high thermal stabilities, high conductivities, and wide electrochemical windows may be potential candidates for use as electrolytes in high-energy density devices. Moreover, this work also sheds some light on the future direction in the search for highly fluid and conductive quaternary ammonium ionic liquids. To further improve the fluidity and conductivity of the quaternary ammonium salts, it is believed that more effort should focus on the development of new stable and weakly coordinating anions with more flexible features than $[C_2F_5BF_3]^-$ and a smaller volume than $[(CF_3SO_2)_2N]^-$ to produce low-melting ionic liquids with very small quaternary ammonium cations.

Experimental Section

General: Commercially available reagents were purchased from Wako Pure Chemicals, Tokyo Kasei, or Aldrich, and used as received. Acidic cation-exchange and basic anion-exchange resins (ion-exchange capacity >2.0 mmol mL^{-1}) were purchased from Mitsubishi Chemicals. Potassium perfluoroalkyltrifluoroborate ($K[R_FBF_3]$ ($R_F = CF_3$, C_2F_5, nC_3F_7, nC_4F_9),[17,37] and *N*-methyloxazolidine[38] were synthesized and purified according to the literature.

^1H, ^{19}F, and ^{11}B NMR spectra were recorded on a JEOL JNM AL400 spectrometer operating at 399.65, 376.05, and 128.15 MHz, respectively. [D$_4$]Methanol was used as the solvent for the bromide salts, and [D$_6$]acetone for the $[R_FBF_3]^-$, $[BF_4]^-$, and $[TFSI]^-$ salts. Chemical shift values are reported relative to TMS as the internal reference (^1H), and to the external references of CCl_3F in [D$_6$]acetone (^{19}F) and $BF_3{\cdot}Et_2O$ in $CDCl_3$ (^{11}B). FAB-MS were measured on a JEOL JMS-HX110/110 A spectrometer. Elemental analysis (C, H, and N) was carried out by the Center for Organic Elemental Microanalysis of Kyoto University.

Water content and impurity: The water content in the room-temperature liquid salts was detected by means of a Karl-Fischer titration (Mitsubishi Chemicals, CA-07). The levels of residual halide and potassium ions in the room-temperature liquid salts were estimated with an X-ray fluorescence spectrometer (JEOL, model JSX-3201).

Phase transition: Calorimetric measurements were performed on a differential scanning calorimeter (Perkin–Elmer Pyris 1 equipped with a liquid nitrogen cooling unit). The temperature calibration was performed with the following standard samples: *n*-pentane (melting point: -132.66 °C), cyclohexane (solid–solid transition: -87.06 °C; melting point: 6.54 °C), *n*-decane (melting point: -29.64 °C), benzoic acid (melting point: 122.37 °C), and indium (melting point: 156.6 °C) used as reference. An average weight of 5–10 mg of each sample was hermetically sealed in an aluminum pan in a dry chamber (Daikin, dew point <-50 °C), and then heated and cooled, both at a rate of 10 °C min^{-1}, under a flow of helium gas. The glass transition temperature (T_g, onset of the heat capacity change), crystallization temperature (T_c, onset of the exothermic peak), solid–solid transition (T_{s-s}, onset of the endothermic peak), and melting point (T_m, onset of the endothermic peak), where appropriate, were recorded on heating in the second heating/cooling cycle for each salt.

Thermal stability: Thermal gravimetric analysis (TGA) was performed on a thermal analysis system (Seiko Instruments, TG/DTA 6200). An average sample weight of 5–10 mg was loaded into a platinum pan and

heated at a rate of 10 °C min^{-1} over a range of approximately 40–600 °C under a slow stream of nitrogen gas. The onset of decomposition was defined as the decomposition temperature (T_d).

Measurements of the density, viscosity, and specific conductivity: The following measurements for the room-temperature liquid salts were carried out in a dry chamber (Daikin, HRG-50 A, dew point < -50 °C). The density (ρ) was measured with a density meter (Anton Paar, DMA-4500) at 25 °C. The reported value for the density is the average of three measurements. The dynamic viscosity (η) was examined by a programmable viscometer (Brookfield, DV-III+) at 25 °C. The specific conductivity (κ) was measured with a conductivity meter (Radiometer Analytical, CDM230) in a cell (Radiometer Analytical, CDC749, cell constant: 1.9 cm^{-1}) at 25 °C. The cell was calibrated with 0.01 M KCl solutions and the data were recorded at a frequency of 23.4 KHz.

Electrochemical stability: Linear-sweep voltammetry was performed on an automatic polarization system (ALS model600) interfaced and monitored with a PC. The ionic liquids were deoxygenated with argon gas prior to the electrochemical measurements. The voltammetric measurements were made in an argon-filled glove box (O_2 and water < 5 ppm) with a standard three-electrode configuration: a glassy carbon electrode (surface area: 7.85×10^{-3} cm^2) served as the working electrode, a Pt wire was used as the counterelectrode, and the reference electrode was a Pt wire immersed in the solutions of 0.015 mol dm^{-3} I_2 + 0.060 mol dm^{-3} $[(nC_3H_7)_4N]I$ in EMI[TFSI] (EMI = 1-ethyl-3-methylimidazolium) and contained in a glass tube with a porous Vycor glass tip. All potentials were given versus the ferrocene (Fc)/ferrocenium (Fc^+) redox couple as the internal standard in each salt. The data for each salt were collected in the first cathodic and anodic scan at 25 °C. The cathodic and anodic limits were arbitrarily defined as the potential at which the current density reached 1.0 mA cm^{-2}. For Li electrodeposition, an Ni electrode (1.77×10^{-3} cm^2) was used as the working electrode to avoid lithium alloy formation, and lithium tetrafluoroborate ($LiBF_4$) dissolved in the ILs (≈ 0.3 mol kg^{-1}) was used as the source of Li^+ ion.

Procedures for the preparation of quaternary ammonium bromide salts ([QA][Br])

***N*-Methoxymethyl-*N*-methylpyrrolidinium bromide ($PY_{1.1O1}Br$)**: Methoxymethyl bromide (25.0 g, 200 mmol) in anhydrous diethyl ether (50 mL) over 30 min was added dropwise to a stirred solution of *N*-methylpyrrolidine (17.5 g, 205 mmol) in anhydrous diethyl ether (50 mL) at 0 °C under an argon atmosphere. The suspension was stirred for 12 h at room temperature. The resulting solid was collected by filtration, washed with diethyl ether (2×25 mL), and dried. The solid was purified by recrystallization from ethanol by addition of diethyl ether to give a white solid. Yield: 82 % (34.4 g); $T_m = 68$ °C; $T_d = 235$ °C; ^{1}H NMR: $\delta = 2.22$ (m, 2×2H), 3.48 (s, 2H), 3.68 (m, 3H, 2H), 4.66 ppm (s, 2H).

***N*-Butyl-*N*-methylpyrrolidinium bromide ($PY_{14}Br$)**: *N*-Methylpyrrolidine (25.6 g, 301 mmol) and 1-bromobutane (41.1 g, 300 mmol) were dissolved in anhydrous acetone (80 mL) in a 500 mL flask at room temperature. The mixture was refluxed for 24 h under an argon atmosphere. After cooling to room temperature, diethyl ether (150 mL) was added to the resulting suspension. The resulting solid was collected by filtration, washed with diethyl ether (2×25 mL), and dried under a high vacuum. The solid was purified by recrystallization from 2-propanol by addition of tetrahydrofuran. White solid; yield: 85 % (56 g); $T_m = 215$ °C; $T_d = 268$ °C; ^{1}H NMR: $\delta = 1.02$ (t, $J = 7.2$ Hz, 3H), 1.43 (m, 2H), 1.80 (m, 2H), 2.24 (brs, 2×2H), 3.09 (s, 3H), 3.40 (m, 2H), 3.57 ppm (brs, 2×2H).

***N*-Methoxyethyl-*N*-methylpyrrolidinium bromide ($PY_{1.1O2}Br$)**: A mixture of *N*-methylpyrrolidine (26.4 g, 0.310 mmol), bromoethyl methyl ether (41.7 g, 300 mmol), and anhydrous acetone (80 mL) in a 500 mL flask was refluxed for 24 h under an argon atmosphere. After evaporation at 70 °C and reduced pressure, the yellow solid was washed with diethyl ether (2×25 mL), followed by recrystallization from 2-butanol by addition of acetone. White solid; yield: 70 % (47.0 g); $T_m = 66$ °C; $T_d = 264$ °C; ^{1}H NMR: $\delta = 2.23$ (s, 2×2H), 3.13 (s, 3H), 3.40 (s, 3H), 3.62 (m, 3×2H), 3.83 ppm (s, 2H).

***N*-Butyl-*N*-methyloxazolidinium bromide ($OX_{14}Br$)**: The salt was prepared under neat conditions following a recently published procedure.[25b] A mixture of *N*-methyloxazolidine[38] (27.0 g, 310 mmol) and 1-bromobutane (41.1 g, 300 mmol) was heated at 70 °C for 24 h under an argon atmosphere. A yellow viscous oil was obtained, which was evaporated at 70 °C under a high vacuum for 24 h to evacuate the volatile materials. After cooling to room temperature, a yellow solid was obtained. The raw product was purified by recrystallization twice from 2-propanol by addition of tetrahydrofuran to afford a white solid (47.5 g, yield 70 %). $T_m = 110$ °C; $T_d = 213$ °C; ^{1}H NMR: $\delta = 1.00$ (t, $J = 7.3$ Hz, 3H), 1.43 (m, 2H), 1.79 (brs, 2H), 3.20 (s, 3H), 3.50 (m, 2H), 3.73–3.80 (2H), 4.36 (m, 2H), 4.88 (s, 1H), 4.95 ppm (s, 1H).

***N*-Methoxyethyl-*N*-methyloxazolidinium bromide ($OX_{1.1O2}Br$)**: The same procedure was followed as that described for the $OX_{14}Br$ salt, except bromoethyl methyl ether (41.7 g, 300 mmol) was used instead of 1-bromobutane. A yellow viscous liquid was obtained that did not crystallize at room temperature. It was dissolved in deionized water (150 mL), extracted with ethyl acetate (2×30 mL), and then decolorized with activated carbon. After filtration, the collected solution was evaporated at 70 °C under reduced pressure to remove water, and then dried at 70 °C under a high vacuum for 24 h to yield a slightly pale yellow liquid (57.6 g, yield 85 %). $T_g = -41$ °C; $T_d = 197$ °C; ^{1}H NMR: $\delta = 3.25$ (s, 3H), 3.41 (t, $J = 5.6$ Hz, 3H), 3.70–3.90 (m, 6H), 4.34 (m, 2H), 4.89 (d, $J = 5.6$ Hz, 1H), 5.01 ppm (d, $J = 5.6$ Hz, 1H).

***N*-Butyl-*N*-methylpiperidinium bromide ($PI_{14}Br$)**: The same procedure was followed as described for the $PY_{14}Br$ salt, except *N*-methylpiperidine (30.0 g, 300 mmol) was used instead of *N*-methylpyrrolidine. The raw product was purified by recrystallization twice from 2-propanol by addition of tetrahydrofuran to afford a white solid (61.0 g, yield 86 %). $T_m = 241$ °C; $T_d = 255$ °C; ^{1}H NMR: $\delta = 1.03$ (t, $J = 7.2$ Hz, 3H), 1.44 (m, 2H), 1.76 (m, 2×2H), 1.92 (brs, 2×2H), 3.08 (s, 3H), 3.40 ppm (m, 3×2H).

***N*-Methoxyethyl-*N*-methylpiperidinium ($PI_{1.1O2}Br$)**: The same procedure was followed as described for the $PY_{1.1O2}Br$ salt, except *N*-methylpiperidine (30.0 g, 300 mmol) was used instead of *N*-methylpyrrolidine. The crude product was purified by recrystallization from 2-butanol by addition of tetrahydrofuran to give a white solid (53.6 g, yield 75 %). $T_m = 132$ °C; $T_d = 254$ °C; ^{1}H NMR: $\delta = 1.70$ (s, 2H), 1.92 (s, 2×2H), 3.17 (m, 3H), 3.38 (s, 3H), 3.48 (m, 2×2H), 3.66 (s, 2H), 3.84 ppm (s, 2H).

***N*-Butyl-*N*-methylmorpholinium bromide ($MO_{14}Br$)**: The same procedure was followed as described for the $OX_{14}Br$ salt, except that *N*-methylmorpholine (31.5 g, 310 mmol) was used instead of *N*-methyloxazolidine. The crude product was purified by recrystallization twice from 1-propanol by addition of tetrahydrofuran to give a white solid (46.4 g, yield 65 %). $T_m = 210$ °C; $T_d = 236$ °C; ^{1}H NMR: $\delta = 1.03$ (t, $J = 7.4$ Hz, 3H), 1.44 (m, 2H), 1.80 (m, 2H), 3.23 (s, 3H), 3.50 (brs, 3×2H), 4.01 ppm (brs, 2×2H).

***N*-Methoxyethyl-*N*-methylmorpholinium bromide ($MO_{1.1O2}Br$)**: The same procedure was followed as described for the $MO_{14}Br$ salt, except bromoethyl methyl ether (41.7 g, 300 mmol) was used instead of 1-bromobutane. The crude product was purified by recrystallization twice from 1-propanol by addition of diethyl ether to give a white solid (46.8 g, yield 65 %). $T_m = 121$ °C; $T_d = 236$ °C; ^{1}H NMR: $\delta = 3.33$ (s, 3H), 3.40 (s, 3H), 3.57 (brm, 2H), 3.63 (brm, 2H), 3.82 (s, 2H), 3.89 (s, 2H), 4.12 ppm (brs, 2×2H).

Procedure for the preparation of aqueous solutions of perfluoroalkyltrifluoroborate acid ($H[R_FBF_3]$) and quaternary ammonium hydroxide ([QA][OH]): Aqueous $H[R_FBF_3]$ and aqueous [QA][OH] were prepared by the respective cation and anion exchange methods, as described in our previous report.[17,20] The solutions were collected in a PFA bottle and stored in a refrigerator until required.

General procedure for the preparation of hydrophobic quaternary ammonium salts with perfluoroalkyltrifluoroborates and bis(trifluoromethanesulfonyl)imide ([QA][R_FBF_3] and [QA][TFSI]): The salts were prepared on a 30 mmol scale. Aqueous [QA][OH] was neutralized with aqueous H[A] ($[A]^- = [(CF_3SO_2)_2N]^-$, and $[R_FBF_3]^-$, $R_F = CF_3$, C_2F_5, nC_3F_7, nC_4F_9) in a PFA flask until the pH was ≈6–7. After concentration to ≈15 mL at 40 °C by evaporation under a vacuum, the liquid salt in the bottom was extracted with CH_2Cl_2 (50 mL), washed with deionized water (2×10 mL), and dried at 70–100 °C for 24 h under a high vacuum to afford a colorless or pale yellow liquid (water content < 50 ppm). The solid salt was collected by filtration, dried under high vacuum, and puri-

fied by recrystallization from 2-propanol or 2-butanol to give a white solid. The characterization data for each salt are presented in the following section. Satisfactory ^{19}F and ^{11}B NMR data for the salts are provided in the Supporting Information. In general, the chemical shift values of ^{19}F and ^{11}B NMR of these cyclic QA salts are nearly the same as those for the related imidazolium or aliphatic QA salts.[20,21]

***N*-Methoxymethyl-*N*-methylpyrrolidinium trifluoromethyltrifluoroborate ($PY_{1.1O1}[CF_3BF_3]$)**: Colorless liquid; yield: 65%; ^1H NMR: $\delta = 2.29$ (m, 2×2H), 3.24 (s, 3H), 3.61 (m, 2H), 3.70 (m, 3H, 2H), 4.78 ppm (s, 2H); FAB-MS: *m/z* (%): 130 (100) $[PY_{1.1O1}]^+$, 137 (100) $[CF_3BF_3]^-$; elemental analysis calcd (%) for $C_8H_{16}BF_6NO$ (267.02): C 35.98, H 6.04, N 5.25; found: C 35.96, H 5.97, N 5.37.

***N*-Butyl-*N*-methylpyrrolidinium trifluoromethyltrifluoroborate ($PY_{14}[CF_3BF_3]$)**: Colorless liquid; yield: 75%; ^1H NMR: $\delta = 0.98$ (t, $J = 7.4$ Hz, 3H), 1.43 (m, 2H), 1.90 (m, 2H), 2.31 (brs, 2×2H), 3.23 (s, 3H), 3.53 (m, 2H), 3.71 ppm (brs, 2×2H); FAB-MS: *m/z* (%): 142 (100) $[PY_{14}]^+$, 137 (100) $[CF_3BF_3]^-$; elemental analysis calcd (%) for $C_{10}H_{20}BF_6N$ (279.07): C 43.04, H 7.22, N 5.02; found: C 42.97, H 7.23, N 5.13.

***N*-Methoxyethyl-*N*-methylpyrrolidinium trifluoromethyltrifluoroborate ($PY_{1.1O2}[CF_3BF_3]$)**: Colorless liquid; yield: 70%; ^1H NMR: $\delta = 2.30$ (s, 2×2H), 3.25 (s, 3H), 3.39 (s, 3H), 3.74 (brs, 3×2H), 3.92 ppm (s, 2H); FAB-MS: *m/z* (%): 144 (100) $[PY_{1.1O2}]^+$, 137 (100) $[CF_3BF_3]^-$; elemental analysis calcd (%) for $C_9H_{18}BF_6NO$ (281.04): C 38.46, H 6.46, N 4.98; found: C 38.18, H 6.29, N 5.25.

***N*-Butyl-*N*-methyloxazolidinium trifluoromethyltrifluoroborate ($OX_{14}[CF_3BF_3]$)**: Colorless liquid; yield: 65%; ^1H NMR: $\delta = 0.99$ (t, $J = 7.4$ Hz, 3H), 1.44 (m, 2H), 1.93 (m, 2H), 3.36 (s, 3H), 3.64 (m, 2H), 3.94 (m, 2H), 4.45 (m, 2H), 5.02 (d, $J = 5.6$ Hz, 1H), 5.08 ppm (d, $J = 5.6$ Hz, 1H); FAB-MS: *m/z* (%): 144 (100) $[OX_{14}]^+$, 137 (100) $[CF_3BF_3]^-$; elemental analysis calcd (%) for $C_9H_{18}BF_6NO$ (281.04): C 38.46, H 6.46, N 4.98; found: C 38.39, H 6.49, N 4.91.

***N*-Methoxyethyl-*N*-methyloxazolidinium trifluoromethyltrifluoroborate ($OX_{1.1O2}[CF_3BF_3]$)**: Pale yellow liquid; yield: 58%; ^1H NMR: $\delta = 3.39$ (s, 3H), 3.41 (s, 3H), 3.90–4.08 (m, 6H), 4.45 (m, 2H), 5.03 (d, $J = 5.60$ Hz, 1H), 5.12 ppm (d, $J = 5.60$ Hz, 1H); FAB-MS: *m/z* (%): 146 (100) $[OX_{1.1O2}]^+$, 137 (100) $[CF_3BF_3]^-$; elemental analysis calcd (%) for $C_8H_{16}BF_6NO_2$ (283.02): C 33.95, H 5.70, N 4.95; found: C 33.66, H 5.67, N 4.91.

***N*-Butyl-*N*-methylpiperidinium trifluoromethyltrifluoroborate ($PI_{14}[CF_3BF_3]$)**: Colorless liquid; yield: 85%; ^1H NMR: $\delta = 0.99$ (t, $J = 7.2$ Hz, 3H), 1.44 (m, 2H), 1.74 (m, 2H), 1.87 (brs, 2H), 1.99 (brs, 2×2H), 3.23 (s, 3H), 3.52 ppm (m, 3×2H); FAB-MS: *m/z* (%): 156 (100) $[PI_{14}]^+$, 137 (100) $[CF_3BF_3]^-$; elemental analysis calcd (%) for $C_{11}H_{22}BF_6N$ (293.10): C 45.08, H 7.57, N 4.78; found: C 45.23, H 7.60, N 4.96.

***N*-Methoxyethyl-*N*-methylpiperidinium trifluoromethyltrifluoroborate ($PI_{1.1O2}[CF_3BF_3]$)**: Colorless liquid; yield: 78%; ^1H NMR: $\delta = 1.73$ (m, 2H), 2.00 (brs, 2×2H), 3.30 (s, 3H), 3.39 (s, 3H), 3.58 (m, 2×2H), 3.78 (m, 2H), 3.95 ppm (s, 2H); FAB-MS: *m/z* (%): 158 (100) $[PI_{1.1O2}]^+$, 137 (100) $[CF_3BF_3]^-$; elemental analysis calcd (%) for $C_{10}H_{20}BF_6NO$ (295.07): C 40.70, H 6.83, N 4.75; found: C 40.75, H 6.95, N 4.94.

***N*-Butyl-*N*-methylmorpholinium trifluoromethyltrifluoroborate ($MO_{14}[CF_3BF_3]$)**: Colorless liquid; yield: 80%; ^1H NMR: $\delta = 0.99$ (t, $J = 7.2$ Hz, 3H), 1.45 (m, 2H), 1.92 (m, 2H), 3.40 (s, 3H), 3.66 (brs, 3×2H), 4.11 ppm (brs, 2×2H); FAB-MS: *m/z* (%): 158 (100) $[MO_{14}]^+$, 137 (100) $[CF_3BF_3]^-$; elemental analysis calcd (%) for $C_{10}H_{20}BF_6NO$ (295.07): C 40.70, H 6.83, N 4.75; found: C 40.61, H 6.81, N 4.74.

***N*-Methoxyethyl-*N*-methylmorpholinium trifluoromethyltrifluoroborate ($MO_{1.1O2}[CF_3BF_3]$)**: Colorless liquid; yield: 75%; ^1H NMR: $\delta = 3.39$ (s, 3H), 3.42 (s, 3H), 3.65 (m, 2H), 3.71 (m, 2H), 3.89 (s, 2H), 3.96 (s, 2H), 4.09 ppm (brs, 2×2H); FAB-MS: *m/z* (%): 160 (100) $[MO_{1.1O2}]^+$, 137 (100) $[CF_3BF_3]^-$; elemental analysis calcd (%) for $C_9H_{18}BF_6NO_2$ (297.04): C 36.39, H 6.11, N 4.72; found: C 36.65, H 6.14, N 4.92.

***N*-Methoxymethyl-*N*-methylpyrrolidinium pentafluoroethyltrifluoroborate ($PY_{1.1O1}[C_2F_5BF_3]$)**: Colorless liquid; yield: 70%; ^1H NMR: $\delta = 2.29$ (m, 2×2H), 3.21 (s, 3H), 3.59 (m, 2H), 3.70 (m, 3H + 2H), 4.78 ppm (s, 2H); FAB-MS: *m/z* (%): 130 (100) $[PY_{1.1O1}]^+$, 187 (100) $[C_2F_5BF_3]^-$; elemental analysis calcd (%) for $C_9H_{16}BF_8NO$ (317.03): C 34.10, H 5.09, N 4.42; found: C 34.37, H 5.08, N 4.40.

***N*-Butyl-*N*-methylpyrrolidinium pentafluoroethyltrifluoroborate ($PY_{14}[C_2F_5BF_3]$)**: Colorless liquid; yield: 89%; ^1H NMR: $\delta = 0.98$ (t, $J = 7.4$ Hz, 3H), 1.43 (m, 2H), 1.91 (m, 2H), 2.32 (brs, 2×2H), 3.25 (s, 3H), 3.54 (m, 2H), 3.72 ppm (brs, 2×2H); FAB-MS: *m/z* (%): 142 (100) $[PY_{14}]^+$, 187 (100) $[C_2F_5BF_3]^-$; elemental analysis calcd (%) for $C_{11}H_{20}BF_8N$ (329.08): C 40.15, H 6.13, N 4.26; found: C 39.94, H 5.82, N 4.20.

***N*-Methoxyethyl-*N*-methylpyrrolidinium pentafluoroethyltrifluoroborate ($PY_{1.1O2}[C_2F_5BF_3]$)**: Colorless liquid; yield: 87%; ^1H NMR: $\delta = 2.31$ (brs, 2×2H), 3.30 (s, 3H), 3.39 (s, 3H), 3.77 (m, 3×2H), 3.94 ppm (s, 2H); FAB-MS: *m/z* (%): 144 (100) $[PY_{1.1O2}]^+$, 187 (100) $[C_2F_5BF_3]^-$; elemental analysis calcd (%) for $C_{10}H_{18}BF_8NO$ (331.05): C 36.28, H 5.48, N 4.23; found: C 36.10, H 5.47, N 4.24.

***N*-Butyl-*N*-methyloxazolidinium pentafluoroethyltrifluoroborate ($OX_{14}[C_2F_5BF_3]$)**: Colorless liquid; yield: 85%; ^1H NMR: $\delta = 0.99$ (t, $J = 7.2$ Hz, 3H), 1.44 (m, 2H), 1.95 (m, 2H), 3.39 (s, 3H), 3.66 (m, 2H), 3.95 (m, 2H), 4.45 (m, 2H), 5.05 (d, $J = 5.6$ Hz, 1H), 5.11 ppm (d, $J = 5.6$ Hz, 1H); FAB-MS: *m/z* (%): 144 (100) $[OX_{14}]^+$, 187 (100) $[C_2F_5BF_3]^-$; elemental analysis calcd (%) for $C_{10}H_{18}BF_8NO$ (333.03): C 36.28, H 5.48, N 4.23; found: C 36.39, H 5.43, N 4.18.

***N*-Methoxyethyl-*N*-methyloxazolidinium pentafluoroethyltrifluoroborate ($OX_{1.1O2}[C_2F_5BF_3]$)**: Pale yellow liquid; yield: 70%; ^1H NMR: $\delta = 3.41$ (s, 3H), 3.42 (s, 3H), 3.90–4.08 (m, 6H), 4.44 (m, 2H), 5.03 (d, $J = 5.6$ Hz, 1H), 5.13 ppm (d, $J = 5.6$ Hz, 1H); FAB-MS: *m/z* (%): 146 (100) $[OX_{1.1O2}]^+$, 187 (100) $[C_2F_5BF_3]^-$; elemental analysis calcd (%) for $C_9H_{16}BF_8NO_2$ (333.03): C 32.46, H 4.84, N 4.21; found: C 32.77, H 4.70, N 4.16.

***N*-Butyl-*N*-methylpiperidinium pentafluoroethyltrifluoroborate ($PI_{14}[C_2F_5BF_3]$)**: White solid; yield: 92%; ^1H NMR: $\delta = 0.99$ (t, $J = 7.2$ Hz, 3H), 1.44 (m, 2H), 1.74 (m, 2H), 1.87 (m, 2H), 2.00 (brs, 2×2H), 3.24 (s, 3H), 3.54 ppm (m, 3×2H); FAB-MS: *m/z* (%): 156 (100) $[PI_{14}]^+$, 187 (100) $[C_2F_5BF_3]^-$; elemental analysis calcd (%) for $C_{12}H_{22}BF_8N$ (343.11): C 42.01, H 6.46, N 4.08; found: C 41.90, H 6.16, N 4.06.

***N*-Methoxyethyl-*N*-methylpiperidinium pentafluoroethyltrifluoroborate ($PI_{1.1O2}[C_2F_5BF_3]$)**: Colorless liquid; yield: 90%; ^1H NMR: $\delta = 1.73$ (m, 2H), 1.97 (brs, 2×2H), 3.26 (s, 3H), 3.38 (s, 3H), 3.60 (m, 2×2H), 3.72 (m, 2H), 3.91 ppm (s, 2H); FAB-MS: *m/z* (%): 158 (100) $[PI_{1.1O2}]^+$, 187 (100) $[C_2F_5BF_3]^-$; elemental analysis calcd (%) for $C_{11}H_{20}BF_8NO$ (345.08): C 38.29, H 5.84, N 4.06; found: C 38.40, H 5.54, N 4.13.

***N*-Butyl-*N*-methylmorpholinium pentafluoroethyltrifluoroborate ($MO_{14}[C_2F_5BF_3]$)**: Colorless liquid; yield: 90%; ^1H NMR: $\delta = 0.99$ (t, $J = 7.2$ Hz, 3H), 1.45 (m, 2H), 1.92 (m, 2H), 3.40 (s, 3H), 3.67 (brs, 3×2H), 4.11 ppm (brs, 2×2H); FAB-MS: *m/z* (%): 158 (100) $[MO_{14}]^+$, 187 (100) $[C_2F_5BF_3]^-$; elemental analysis calcd (%) for $C_{11}H_{20}BF_8NO$ (345.08): C 38.29, H 5.84, N 4.06; found: C 38.21, H 5.82, N 3.97.

***N*-Methoxyethyl-*N*-methylmorpholinium pentafluoroethyltrifluoroborate ($MO_{1.1O2}[C_2F_5BF_3]$)**: Colorless liquid; yield: 82%; ^1H NMR: $\delta = 3.39$ (s, 3H), 3.45 (s, 3H), 3.68 (m, 2H), 3.74 (m, 2H), 3.93 (s, 2H), 3.99 (s, 2H), 4.10 ppm (brs, 2×2H); FAB-MS: *m/z* (%): 160 (100) $[MO_{1.1O2}]^+$, 187 (100) $[C_2F_5BF_3]^-$; elemental analysis calcd (%) for $C_{10}H_{18}BF_8NO_2$ (347.05): C 34.61, H 5.23, N 4.04; found: C 34.31, H 5.14, N 4.05.

***N*-Butyl-*N*-methylpyrrolidinium (heptafluoro-*n*-propyl)trifluoroborate ($PY_{14}[nC_3F_7BF_3]$)**: White solid; yield: 92%; ^1H NMR: $\delta = 0.98$ (t, $J = 7.2$ Hz, 3H), 1.44 (m, 2H), 1.90 (brs, 2H), 2.31 (brs, 2×2H), 3.23 (s, 3H), 3.52 (m, 2H), 3.70 ppm (brs, 2×2H); FAB-MS: *m/z* (%): 142 (100) $[PY_{14}]^+$, 237 (100) $[C_3F_7BF_3]^-$; elemental analysis calcd (%) for $C_{12}H_{20}BF_{10}N$ (379.09): C 38.02, H 5.32, N 3.69; found: C 37.84, H 5.20, N 3.80.

***N*-Methoxyethyl-*N*-methylpyrrolidinium (heptafluoro-*n*-propyl)trifluoroborate ($PY_{1.1O2}[nC_3F_7BF_3]$)**: Colorless liquid; yield: 87%; ^1H NMR: $\delta =$ 2.30 (brs, 2×2H), 3.27 (s, 3H), 3.40 (s, 3H), 3.75 (m, 3×2H), 3.92 ppm (s, 2H); FAB-MS: *m/z* (%): 144 (100) $[PY_{1.1O2}]^+$, 237 (100) $[C_3F_7BF_3]^-$; elemental analysis calcd (%) for $C_{11}H_{18}BF_{10}NO$ (381.06): C 34.67, H 4.76, N 3.68; found: C 34.89, H 4.56, N 3.72.

***N*-Butyl-*N*-methyloxazolidinium (heptafluoro-*n*-propyl)trifluoroborate ($OX_{14}[nC_3F_7BF_3]$)**: White solid; yield: 87%; ^1H NMR: $\delta = 0.99$ (t, $J =$

7.4 Hz, 3H), 1.44 (m, 2H), 1.95 (m, 2H), 3.40 (s, 3H), 3.66 (m, 2H), 3.95 (m, 2H), 4.48 (m, 2H), 5.05 (d, $J=5.6$ Hz, 1H), 5.11 ppm (d, $J=5.6$ Hz, 1H); FAB-MS: m/z (%): 144 (100) $[OX_{14}]^+$, 237 (100) $[C_3F_7BF_3]^-$; elemental analysis calcd (%) for $C_{11}H_{18}BF_{10}NO$ (381.06): C 34.67, H 4.76, N 3.68; found: C 34.40, H 4.69, N 3.66.

***N*-Methoxyethyl-*N*-methyloxazolidinium (heptafluoro-*n*-propyl)trifluoroborate ($OX_{1.1O2}[nC_3F_7BF_3]$)**: Pale yellow liquid; yield: 82%; ^{1}H NMR: $\delta=3.39$ (s, 3H), 3.41 (s, 3H), 3.90–4.04 (m, 6H), 4.45 (m, 2H), 5.03 (d, $J=5.6$ Hz, 1H), 5.12 ppm (d, $J=5.6$ Hz, 1H); FAB-MS: m/z (%): 146 (100) $[OX_{1.1O2}]^+$, 237 (100) $[C_3F_7BF_3]^-$; elemental analysis calcd (%) for $C_{10}H_{16}BF_{10}NO_2$ (383.04): C 31.36, H 4.21, N 3.66; found: C 31.16, H 4.07, N 3.77.

***N*-Butyl-*N*-methylpiperidinium (heptafluoro-*n*-propyl)trifluoroborate ($PI_{14}[nC_3F_7BF_3]$)**: White solid; yield: 95%; ^{1}H NMR: $\delta=0.99$ (t, $J=7.2$ Hz, 3H), 1.44 (m, 2H), 1.74 (m, 2H), 1.87 (m, 2H), 2.00 (brs, 2×2H), 3.24 (s, 3H), 3.54 ppm (m, 3×2H); FAB-MS: m/z (%): 156 (100) $[PI_{14}]^+$, 237 (100) $[C_3F_7BF_3]^-$; elemental analysis calcd (%) for $C_{13}H_{22}BF_{10}N$: C 39.72, H 5.64, N 3.56; found: C 39.44, H 5.56, N 3.82.

***N*-Methoxyethyl-*N*-methylpiperidinium (heptafluoro-*n*-propyl)trifluoroborate ($PI_{1.1O2}[nC_3F_7BF_3]$)**: Colorless liquid; yield: 91%; ^{1}H NMR: $\delta=$ 1.73 (m, 2H), 1.99 (brs, 2×2H), 3.30 (s, 3H), 3.38 (s, 3H), 3.60 (m, 2× 2H), 3.77 (m, 2H), 3.94 ppm (s, 2H); FAB-MS: m/z (%): 158 (100) $[PI_{1.1O2}]^+$, 237 (100) $[C_3F_7BF_3]^-$; elemental analysis calcd (%) for $C_{12}H_{20}BF_{10}NO$ (393.12): C 36.48, H 5.10, N 3.55; found: C 36.18, H 4.88, N 3.59.

***N*-Butyl-*N*-methylmorpholinium (heptafluoro-*n*-propyl)trifluoroborate ($MO_{14}[nC_3F_7BF_3]$)**: White solid; yield: 90%; ^{1}H NMR: $\delta=1.00$ (t, $J=$ 7.2 Hz, 3H), 1.45 (m, 2H), 1.91 (m, 2H), 3.39 (s, 3H), 3.67 (m, 3×2H), 4.10 ppm (brs, 2×2H); FAB-MS: m/z (%): 158 (100) $[MO_{14}]^+$, 237 (100) $[C_3F_7BF_3]^-$; elemental analysis calcd (%) for $C_{12}H_{20}BF_{10}NO$ (395.09): C 36.48, H 5.10, N 3.55; found: C 36.33, H 5.10, N 3.48.

***N*-Methoxyethyl-*N*-methylmorpholinium (heptafluoro-*n*-propyl)trifluoroborate ($MO_{1.1O2}[nC_3F_7BF_3]$)**: Colorless liquid; yield: 90%; ^{1}H NMR: $\delta=$ 3.39 (s, 3H), 3.45 (s, 3H), 3.68 (m, 2H), 3.73 (m, 2H), 3.92 (s, 2H), 3.98 (s, 2H), 4.09 ppm (brs, 2×2H); FAB-MS: m/z (%): 160 (100) $[MO_{1.1O2}]^+$, 237 (100) $[C_3F_7BF_3]^-$; elemental analysis calcd (%) for $C_{11}H_{18}BF_{10}NO_2$ (397.06): C 33.27, H 4.57, N 3.53; found: C 33.01, H 4.31, N 3.61.

***N*-Butyl-*N*-methylpyrrolidinium (nonafluoro-*n*-butyl)trifluoroborate ($PY_{14}[nC_4F_9BF_3]$)**: White solid; yield: 95%; ^{1}H NMR: $\delta=0.98$ (t, $J=$ 7.4 Hz, 3H), 1.43 (m, 2H), 1.90 (m, 2H), 2.31 (brs, 2×2H), 3.22 (s, 3H), 3.52 (m, 2H), 3.70 ppm (brs, 2×2H); FAB-MS: m/z (%): 142 (100) $[PY_{14}]^+$, 287 (100) $[C_4F_9BF_3]^-$; elemental analysis calcd (%) for $C_{13}H_{20}BF_{12}N$: C 36.39, H 4.70, N 3.26; found: C 36.11, H 4.66, N 3.47.

***N*-Methoxyethyl-*N*-methylpyrrolidinium (nonafluoro-*n*-butyl)trifluoroborate ($PY_{1.1O2}[nC_4F_9BF_3]$)**: Colorless liquid; yield: 95%; ^{1}H NMR: $\delta=2.30$ (brs, 2×2H), 3.27 (s, 3H), 3.40 (s, 3H), 3.75 (brs, 3×2H), 3.92 ppm (s, 2H); FAB-MS: m/z (%): 144 (100) $[PY_{1.1O2}]^+$, 287 (100) $[C_4F_9BF_3]^-$; elemental analysis calcd (%) for $C_{12}H_{18}BF_{12}NO$ (429.10): C 33.44, H 4.21, N 3.25; found: C 33.18, H 4.02, N 3.45.

***N*-Butyl-*N*-methyloxazolidinium (nonafluoro-*n*-butyl)trifluoroborate ($OX_{14}[nC_4F_9BF_3]$)**: White solid; yield: 91%; ^{1}H NMR: $\delta=0.99$ (t, $J=$ 7.4 Hz, 3H), 1.44 (m, 2H), 1.93 (m, 2H), 3.37 (s, 3H), 3.64 (m, 2H), 3.95 (m, 2H), 4.45 (m, 2H), 5.03 (d, $J=5.6$ Hz, 1H), 5.10 ppm (d, $J=5.6$ Hz, 1H); FAB-MS: m/z (%): 144 (100) $[OX_{14}]^+$, 287 (100) $[C_4F_9BF_3]^-$; elemental analysis calcd (%) for $C_{12}H_{18}BF_{12}NO$ (431.07): C 33.44, H 4.21, N 3.25; found: C 32.45, H 3.97, N 3.19.

***N*-Methoxyethyl-*N*-methyloxazolidinium (nonafluoro-*n*-butyl)trifluoroborate ($OX_{1.1O2}[nC_4F_9BF_3]$)**: Pale yellow liquid; yield: 85%; ^{1}H NMR: $\delta=$ 3.41 (s, 3H), 3.42 (s, 3H), 3.90–4.08 (m, 6H), 4.44 (m, 2H), 5.03 (d, $J=$ 5.6 Hz, 1H), 5.13 ppm (d, $J=5.6$ Hz, 1H); FAB-MS: m/z (%): 146 (100) $[OX_{1.1O2}]^+$, 287 (100) $[C_4F_9BF_3]^-$; elemental analysis calcd (%) for $C_{11}H_{16}BF_{12}NO_2$ (433.05): C 30.51, H 3.72, N 3.23; found: C 30.49, H 3.73, N 3.35.

***N*-Butyl-*N*-methylpiperidinium (nonafluoro-*n*-butyl)trifluoroborate ($PI_{14}[nC_4F_9BF_3]$)**: White solid; yield: 95%; ^{1}H NMR: $\delta=0.99$ (t, $J=7.2$ Hz, 3H), 1.44 (m, 2H), 1.74 (m, 2H), 1.87 (m, 2H), 1.99 (brs, 2×2H); 3.23 (s, 3H), 3.53 ppm (m, 3×2H); FAB-MS: m/z (%): 156 (100) $[PI_{14}]^+$, 287 (100) $[C_4F_9BF_3]^-$; elemental analysis calcd (%) for $C_{14}H_{22}BF_{12}N$ (443.13): C 37.95, H 5.00, N 3.16; found: C 37.70, H 4.94, N 3.19.

***N*-Methoxyethyl-*N*-methylpiperidinium (nonafluoro-*n*-butyl)trifluoroborate ($PI_{1.1O2}[nC_4F_9BF_3]$)**: Colorless liquid; yield: 93%; ^{1}H NMR: $\delta=1.73$ (m, 2H), 2.00 (brs, 2×2H), 3.30 (s, 3H), 3.39 (s, 3H), 3.60 (m, 2×2H), 3.78 (m, 2H), 3.95 ppm (s, 2H); FAB-MS: m/z (%): 158 (100) $[PI_{1.1O2}]^+$, 287 (100) $[C_4F_9BF_3]^-$; elemental analysis calcd (%) for $C_{13}H_{20}BF_{12}NO$ (445.10): C 35.08, H 4.53, N 3.15; found: C 35.13, H 4.35, N 3.44.

***N*-Butyl-*N*-methylmorpholinium (nonafluoro-*n*-butyl)trifluoroborate ($MO_{14}[nC_4F_9BF_3]$)**: White solid; yield: 94%; ^{1}H NMR: $\delta=1.00$ (t, $J=$ 7.4 Hz, 3H), 1.45 (m, 2H), 1.91 (m, 2H), 3.40 (s, 3H), 3.67 (m, 3×2H), 4.11 ppm (brs, 2×2H); FAB-MS: m/z (%): 158 (100) $[MO_{14}]^+$, 287 (100) $[C_4F_9BF_3]^-$; elemental analysis calcd (%) for $C_{13}H_{20}BF_{12}NO$ (445.10): C 35.08, H 4.53, N 3.15; found: C 34.79, H 4.33, N 3.30.

***N*-Methoxyethyl-*N*-methylmorpholinium (nonafluoro-*n*-butyl)trifluoroborate ($MO_{1.1O2}[nC_4F_9BF_3]$)**: Yield 90%, white solid; ^{1}H NMR: $\delta=3.39$ (s, 3H), 3.44 (s, 3H), 3.67 (m, 2H), 3.73 (m, 2H), 3.91 (s, 2H), 3.97 (s, 2H), 4.09 ppm (brs, 2×2H); FAB-MS: m/z (%): 160 (100) $[MO_{1.1O2}]^+$, 287 (100) $[C_4F_9BF_3]^-$; elemental analysis calcd (%) for $C_{12}H_{18}BF_{12}NO_2$ (447.07): C 32.24, H 4.06, N 3.13; found: C 32.29, H 4.23, N 3.18.

***N*-Methoxymethyl-*N*-methylpyrrolidinium bis(trifluoromethanesulfonyl)imide ($PY_{1.1O1}[TFSI]$)**: Colorless liquid; yield: 85%; ^{1}H NMR: $\delta=2.29$ (m, 2×2H), 3.25 (s, 3H), 3.62 (m, 2H), 3.72 (s, 3H), 3.74 (m, 2H), 4.79 ppm (s, 2H); FAB-MS: m/z (%): 130 (100) $[PY_{1.1O1}]^+$, 280 (100) $[TFSI]^-$; elemental analysis calcd (%) for $C_9H_{16}F_6N_2O_5S_2$ (410.36): C 26.34, H 3.93, N 6.83; found: C 26.38, H 3.91, N 7.02.

***N*-Butyl-*N*-methylpyrrolidinium bis(trifluoromethanesulfonyl)imide ($PY_{14}[TFSI]$)**: Colorless liquid; yield: 94%; ^{1}H NMR: $\delta=0.99$ (t, $J=$ 7.4 Hz, 3H), 1.43 (m, 2H), 1.90 (m, 2H), 2.32 (brs, 2×2H), 3.27 (s, 3H), 3.55 (m, 2H), 3.73 ppm (brs, 2×2H); FAB-MS: m/z (%): 142 (100) $[PY_{14}]^+$, 280 (100) $[TFSI]^-$; elemental analysis calcd (%) for $C_{11}H_{20}F_6N_2O_4S_2$ (422.41): C 31.28, H 4.77, N 6.63; found: C 31.30, H 4.47, N 6.72.

***N*-Methoxyethyl-*N*-methylpyrrolidinium bis(trifluoromethanesulfonyl)imide ($PY_{1.1O2}[TFSI]$)**: Colorless liquid; yield: 93%; ^{1}H NMR: $\delta=2.32$ (brs, 2×2H), 3.30 (brs, 3H), 3.40 (s, 3H), 3.79 (brs, 3×2H), 3.95 ppm (s, 2H); FAB-MS: m/z (%): 144 (100) $[PY_{1.1O2}]^+$, 280 (100) $[TFSI]^-$; elemental analysis calcd (%) for $C_{10}H_{18}F_6N_2O_5S_2$ (424.38): C 28.30, H 4.28, N 6.60; found: C 28.41, H 4.20, N 6.60.

***N*-Butyl-*N*-methyloxazolidinium bis(trifluoromethanesulfonyl)imide ($OX_{14}[TFSI]$)**: Colorless liquid; yield: 90%; ^{1}H NMR: $\delta=0.99$ (t, $J=$ 7.6 Hz, 3H), 1.45 (m, 2H), 1.95 (m, 2H), 3.40 (s, 3H), 3.67 (m, 2H), 3.97 (m, 2H), 4.46 (m, 2H), 5.06 (d, $J=5.6$ Hz, 1H), 5.12 ppm (d, $J=5.6$ Hz, 1H); elemental analysis calcd (%) for $C_{10}H_{18}F_6N_2O_5S_2$ (424.38): C 28.30, H 4.28, N 6.60; found: C 28.15, H 4.23, N 6.65.

***N*-Methoxyethyl-*N*-methyloxazolidinium bis(trifluoromethanesulfonyl)imide ($OX_{1.1O2}[TFSI]$)**: Pale yellow liquid; yield: 86%; ^{1}H NMR: $\delta=3.42$ (s, 3H), 3.44 (s, 3H), 3.95–4.08 (m, 6H), 4.45 (m, 2H), 5.05 (d, $J=$ 5.60 Hz, 1H), 5.16 ppm (d, $J=5.60$ Hz, 1H); elemental analysis calcd (%) for $C_9H_{16}F_6N_2O_6S_2$ (426.36): C 25.35, H 3.78, N 6.57; found: C 25.38, H 3.75, N 6.63.

***N*-Butyl-*N*-methylpiperidinium bis(trifluoromethanesulfonyl)imide ($PI_{14}[TFSI]$)**: Colorless liquid; yield: 96%; ^{1}H NMR: $\delta=0.99$ (t, $J=7.2$ Hz, 3H), 1.44 (m, 2H), 1.74 (m, 2H), 1.86 (m, 2H), 2.00 (brs, 2×2H), 3.24 (s, 3H), 3.55 ppm (m, 3×2H); FAB-MS: m/z (%): 156 (100) $[PI_{14}]^+$, 280 (100) $[TFSI]^-$; elemental analysis calcd (%) for $C_{12}H_{22}F_6N_2O_4S_2$ (436.44): C 33.02, H 5.08, N 6.42; found: C 33.19, H 4.80, N 6.43.

***N*-Methoxyethyl-*N*-methylpiperidinium bis(trifluoromethanesulfonyl)imide ($PI_{1.1O2}[TFSI]$)**: Colorless liquid; yield: 91%; ^{1}H NMR: $\delta=1.74$ (brs, 2H), 1.97 (brs, 2×2H), 3.33 (s, 3H), 3.39 (s, 3H), 3.64 (m, 2×2H), 3.72 (s, 2H), 3.91 ppm (s, 2H); FAB-MS: m/z (%): 158 (100) $[PI_{1.1O2}]^+$, 280 (100) $[TFSI]^-$; elemental analysis calcd (%) for $C_{11}H_{20}F_6N_2O_5S2$ (438.41): C 30.14, H 4.60, N 6.39; found: C 30.41, H 4.31, N 6.47.

***N*-Butyl-*N*-methylmorpholinium bis(trifluoromethanesulfonyl)imide ($MO_{14}[TFSI]$)**: Colorless liquid; yield: 90%; ^{1}H NMR: $\delta=1.00$ (t, $J=$ 7.2 Hz, 3H), 1.45 (m, 2H), 1.92 (m, 2H), 3.41 (s, 3H), 3.67 (m, 3×2H), 4.11 ppm (brs, 2×2H); FAB-MS: m/z (%): 158 (100) $[MO_{14}]^+$, 280 (100)

[TFSI]$^-$; elemental analysis calcd (%) for $C_{11}H_{20}F_6N_2O_5S_2$ (438.41): C 30.14, H 4.60, N 6.39; found: C 30.01, H 4.58, N 6.37.

***N*-Methoxyethyl-*N*-methylmorpholinium bis(trifluoromethanesulfonyl)-imide ($MO_{1.1O2}$[TFSI])**: Colorless liquid; yield: 89%; ^{1}H NMR: $\delta = 3.39$ (s, 3H), 3.48 (s, 3H), 3.70 (m, 2H), 3.76 (m, 2H), 3.95 (s, 2H), 3.99 (s, 2H), 4.11 ppm (brs, 2×2H); FAB-MS: *m*/*z* (%): 160 (100) $[MO_{1.1O2}]^+$, 280 (100) [TFSI]$^-$; elemental analysis calcd (%) for $C_{10}H_{18}F_6N_2O_6S_2$ (440.38): C 27.27, H 4.12, N 6.36; found: C 27.15, H 3.84, N 6.44.

General procedure for hydrophilic quaternary ammonium salts with tetrafluoroborate ([QA][BF_4]): The salts were prepared on a 50 mmol scale as follows. The aqueous [QA][OH] was neutralized with aqueous H[BF_4] in a PFA flask to a pH value of 6–7. The solution was concentrated at 30–40 °C at reduced pressure, giving a viscous liquid or a solid. The viscous liquid was further dried at 40 °C for 24 h under high vacuum to remove the volatile impurities and then dissolved in anhydrous CH_2Cl_2 (60 mL), filtered through a PTFE membrane filter (0.2 μm). The collected solution was evaporated, and dried at 70–100 °C for 48 h under a high vacuum to give a pale yellow or colorless liquid (water content: ≈100–300 ppm). The solid product was dried at 90 °C and purified by recrystallization from methanol on addition of 2-butanol to give a white solid.

***N*-Methoxymethyl-*N*-methylpyrrolidinium tetrafluoroborate ($PY_{1.1O1}$-[BF_4])**: Colorless liquid; yield: 95%; ^{1}H NMR: $\delta = 2.26$ (m, 2×2H), 3.20 (s, 3H), 3.59 (m, 2H), 3.71 (m, 3H + 2H), 4.77 ppm (s, 2H); FAB-MS: *m*/*z* (%): 130 (100) $[PY_{1.1O1}]^+$, 87 (100) $[BF_4]^-$; elemental analysis calcd (%) for $C_7H_{16}BF_4NO$ (217.02): C 38.74, H 7.43, N 6.45; found: C 38.94, H 7.45, N 6.46.

***N*-Butyl-*N*-methylpyrrolidinium tetrafluoroborate (PY_{14}[BF_4])**: White solid; yield: 90%; ^{1}H NMR: $\delta = 0.98$ (t, $J = 7.4$ Hz, 3H), 1.43 (m, 2H), 1.89 (brs, 2H), 2.30 (brs, 2×2H), 3.24 (s, 3H), 3.52 (m, 2H), 3.71 ppm (brs, 2×2H); FAB-MS: *m*/*z* (%): 142 (100) $[PY_{14}]^+$, 87 (100) $[BF_4]^-$; elemental analysis calcd (%) for $C_9H_{20}BF_4N$ (229.07): C 47.19, H 8.80, N 6.11; found: C 47.02, H 8.95, N 6.14.

***N*-Methoxyethyl-*N*-methylpyrrolidinium tetrafluoroborate ($PY_{1.1O2}$[BF_4])**: Pale yellow liquid; yield: 96%; ^{1}H NMR: $\delta = 2.31$ (brs, 2×2H), 3.30 (s, 3H), 3.39 (s, 3H), 3.77 (m, 3×2H), 3.94 ppm (s, 2H); FAB-MS: *m*/*z* (%): 144 (100) $[PY_{1.1O2}]^+$, 87 (100) $[BF_4]^-$; elemental analysis calcd (%) for $C_8H_{18}BF_4NO$ (231.04): C 41.59, H 7.85, N 6.06; found: C 41.77, H 8.05, N 6.34.

***N*-Butyl-*N*-methyloxazolidinium tetrafluoroborate (OX_{14}[BF_4])**: Pale yellow liquid; yield: 95%; ^{1}H NMR: $\delta = 0.99$ (t, $J = 7.4$ Hz, 3H), 1.44 (m, 2H), 1.92 (m, 2H), 3.33 (s, 3H), 3.63 (m, 2H), 3.91 (m, 2H), 4.43 (m, 2H), 5.01 (d, $J = 5.6$ Hz, 1H), 5.08 ppm (d, $J = 5.6$ Hz, 1H); FAB-MS: *m*/*z* (%): 144 (100) $[OX_{14}]^+$, 87 (100) $[BF_4]^-$; elemental analysis calcd (%) for $C_8H_{18}BF_4NO$ (231.04): C 41.59, H 7.85, N 6.06; found: C 41.39, H 7.59, N 6.17.

***N*-Methoxyethyl-*N*-methyloxazolidinium tetrafluoroborate ($OX_{1.1O2}$-[BF_4])**: Pale yellow liquid; yield: 94%; ^{1}H NMR: $\delta = 3.40$ (s, 3H), 3.42 (s, 3H), 3.88–4.07 (m, 6H), 4.45 (m, 2H), 5.02 (d, $J = 5.6$ Hz, 1H), 5.12 ppm (d, $J = 5.6$ Hz, 1H); FAB-MS: *m*/*z* (%): 146 (100) $[OX_{1.1O2}]^+$, 87 (100) $[BF_4]^-$; elemental analysis calcd (%) for $C_7H_{16}BF_4NO_2$ (233.02): C 36.08, H 6.92, N 6.01; found: C 35.92, H 6.63, N 6.22.

***N*-Butyl-*N*-methylpiperidinium tetrafluoroborate (PI_{14}[BF_4])**: White solid; yield: 88%; ^{1}H NMR: $\delta = 0.99$ (t, $J = 7.2$ Hz, 3H), 1.43 (m, 2H), 1.74 (m, 2H), 1.86 (m, 2H), 1.99 (brs, 2×2H), 3.23 (s, 3H), 3.53 ppm (m, 3×2H); FAB-MS: *m*/*z* (%): 156 (100) $[PI_{14}]^+$, 87 (100) $[BF_4]^-$; elemental analysis calcd (%) for $C_{10}H_{22}BF_4N$ (243.10): C 49.41, H 9.12, N 5.76; found: C 49.38, H 8.82, N 5.74.

***N*-Methoxyethyl-*N*-methylpiperidinium tetrafluoroborate ($PI_{1.1O2}$[BF_4])**: Colorless liquid; yield: 94%; ^{1}H NMR: $\delta = 1.73$ (m, 2H), 2.00 (brs, 2×2H), 3.30 (s, 3H), 3.39 (s, 3H), 3.60 (m, 2×2H), 3.78 (m, 2H), 3.95 ppm (s, 2H); FAB-MS: *m*/*z* (%): 158 (100) $[PI_{1.1O2}]^+$, 87 (100) $[BF_4]^-$; elemental analysis calcd (%) for $C_9H_{20}BF_4NO$ (245.07): C 44.11, H 8.23, N 5.72; found: C 44.15, H 8.01, N 5.75.

***N*-Butyl-*N*-methylmorpholinium tetrafluoroborate (MO_{14}[BF_4])**: White solid; yield: 89%; ^{1}H NMR: $\delta = 0.99$ (t, $J = 7.4$ Hz, 3H), 1.45 (m, 2H), 1.89 (m, 2H), 3.37 (s, 3H), 3.65 (m, 3×2H), 4.08 ppm (brs, 2×2H); FAB-MS: *m*/*z* (%): 158 (100) $[MO_{14}]^+$, 87 (100) $[BF_4]^-$; elemental analysis calcd (%) for $C_9H_{20}BF_4NO$ (245.07): C 44.11, H 8.23, N 5.72; found: C 44.18, H 8.33, N 5.74.

***N*-Methoxyethyl-*N*-methylmorpholinium tetrafluoroborate ($MO_{1.1O2}$-[BF_4])**: White solid; yield: 88%; ^{1}H NMR: $\delta = 3.39$ (s, 3H), 3.43 (s, 3H), 3.66 (m, 2H), 3.71 (m, 2H), 3.90 (s, 2H), 3.96 (s, 2H), 4.08 ppm (brs, 2×2H); FAB-MS: *m*/*z* (%): 160 (100) $[MO_{1.1O2}]^+$, 87 (100) $[BF_4]^-$; elemental analysis calcd (%) for $C_8H_{18}BF_4NO_2$ (247.04): C 38.89, H 7.34, N 5.67; found: C 38.90, H 7.06, N 5.71.

Acknowledgements

This work was supported by Grant-in-Aid for Scientific Research from the Japanese Ministry of Education, Science, Sports, and Culture (No. 17073017).

[1] For books, see: a) P. Wasserscheid, T. Welton, *Ionic Liquids in Synthesis*, Wiley-VCH, Weinheim, **2003**; b) R. D. Rogers, K. R. Seddon, *Ionic Liquids: Industrial Applications for Green Chemistry* (ACS Symposium Series 818), American Chemical Society, Washington, DC, **2002**; c) R. D. Rogers, K. R. Seddon, *Ionic Liquids as Green Solvents: Progress and Prospects* (ACS Symposium Series 856), American Chemical Society, Washington, DC, **2003**; d) R. D. Rogers, K. R. Seddon, *Ionic Liquids IIIA: Fundamentals, Progress, Challenges, and Opportunities* (ACS Symposium Series 901), American Chemical Society, Washington, DC, **2005**; e) R. D. Rogers, K. R. Seddon, *Ionic Liquids IIIB: Fundamentals, Progress, Challenges, and Opportunities* (ACS Symposium Series 902), American Chemical Society, Washington, DC, **2005**.

[2] For selected reviews, see: a) T. Welton, *Chem. Rev.* **1999**, *99*, 2071–2084; b) P. Wasserscheid, W. Keim, *Angew. Chem.* **2000**, *112*, 3926–3945; *Angew. Chem. Int. Ed.* **2000**, *39*, 3772–3789; c) J. Dupont, R. F. de Souza, P. A. Z. Suarez, *Chem. Rev.* **2002**, *102*, 3667–3692.

[3] For selected reviews, see: a) R. A. Sheldon, R. M. Lau, M. J. Sorgedrager, F. van-Rantwijk, K. R. Seddon, *Green Chem.* **2002**, *4*, 147–151; b) U. Kragel, M. Eckstein, N. Kaftzik, *Curr. Opin. Biotechnol.* **2002**, *13*, 565–571; c) S. Park, R. J. Kazlauskas, *Curr. Opin. Biotechnol.* **2003**, *14*, 432–437.

[4] For selected reviews, see: a) C. C. Tzschucke, C. Markert, W. Bannwarth, S. Roller, A. Hebel, R. Haag, *Angew. Chem.* **2002**, *114*, 4136–4173; *Angew. Chem. Int. Ed.* **2002**, *41*, 3964–4000; b) C. F. Poole, *J. Chromatogr. A* **2004**, *1037*, 49–82.

[5] a) M. Antonietti, D. Kuang, B. Smarsly, Y. Zhou, *Angew. Chem.* **2004**, *116*, 5096–5100; *Angew. Chem. Int. Ed.* **2004**, *43*, 4988–4992; b) E. R. Cooper, C. D. Andrews, P. S. Wheatley, P. B. Webb, P. Wormald, R. E. Morris, *Nature* **2004**, *430*, 1012–1016.

[6] For books, see: a) H. Ohno, *Electrochemical Aspects of Ionic Liquids*, Wiley-Interscience, Hoboken/New Jersey, **2005**; b) A. Weber, G. E. Blomgrem in *Advances in Lithium-Ion Batteries* (Eds.: W. A. Van Schalkwijk, B. Scrosati), Kluwer Academic/Plenum, New York, **2002**, pp. 185–232.

[7] For examples of imidazolium ionic liquids, see: a) N. Nakagawa, S. Izuchi, K. Kuwana, T. Nukuda, Y. Aihara, *J. Electrochem. Soc.* **2003**, *150*, A695–A700; b) B. Garcia, S. Lavallee, G. Perron, C. Michot, M. Armand, *Electrochim. Acta* **2004**, *49*, 4583–4588.

[8] For examples of quaternary ammonium ionic liquids, see: a) H. Sakaebe, H. Matsumoto, *Electrochem. Commun.* **2003**, *5*, 594–598; b) J. H. Shin, W. A. Henderson, S. Passerini, *Electrochem. Commun.* **2003**, *5*, 1016–1020; c) T. Sato, T. Maruo, S. Marukane, K. Takagi, *J. Power Sources* **2004**, *138*, 253–261; d) H. Matsumoto, H. Sakaebe, K. Tatsumi, *J. Power Sources* **2005**, *146*, 45–50.

[9] a) M. Ue, M. Takeda, A. Toriumi, A. Kominato, R. Hagiwara, Y. Ito, *J. Electrochem. Soc.* **2003**, *150*, 499–502; b) Y. J. Kim, Y. Matsuzawa, S. Ozaki, K. C. Park, C. Kim, M. Endo, H. Yoshida, G. Masuda, T. Sato, M. S. Dresselhausc, *J. Electrochem. Soc.* **2005**, *152*, A710–A715.

[10] a) A. Noda, M. A. B. H. Susan, K. Kudo, S. Mitsushima, K Hayamizu, M. Watanabe, *J. Phys. Chem. B* **2003**, *107*, 4024–4033; b) M. Yoshizawa, W. Xu, C. A. Angell, *J. Am. Chem. Soc.* **2003**, *125*, 15411–15419; c) R. F. de Souza, J. C. Padilha, R. S. Goncalves, J. Dupont, *Electrochem. Commun.* **2003**, *5*, 728–731.
[11] a) A. I. Bhatt, I. May, V. A. Volkovich, M. E. Hetherington, B. Lewin, R. C. Thied, N. Ertokc, *J. Chem. Soc. Dalton Trans.* **2002**, 4532–4534; b) A. I. Bhatt, I. May, V. A. Volkovich, D. Collison, M. Helliwell, I. B. Polovov, R. G. Lewin, *Inorg. Chem.* **2005**, *44*, 4934–4940.
[12] K. Xu, *Chem. Rev.* **2004**, *104*, 4303–4417.
[13] P. C. Howlett, D. R. MacFarlane, A. F. Hollenkamp, *Electrochem. Solid-State Lett.* **2004**, *7*, A97–A101.
[14] a) J. Sun, M. Forsyth, D. R. MacFarlane, *Ionics* **1997**, *3*, 356–362; b) J. Sun, M. Forsyth, D. R. MacFarlane, *J. Phys. Chem. B* **1998**, *102*, 8858–8864.
[15] a) D. R. MacFarlane, P. Meakin, J. Sun, N. Amini, M. Forsyth, *J. Phys. Chem. A* **1999**, *103*, 4164–4170; b) D. R. McFarlane, J. Sun, J. Golding, P. Meakin, M. Forsyth, *Electrochim. Acta* **2000**, *45*, 1271–1278.
[16] H. Matsumoto, M. Yanagida, K. Tanimoto, M. Nomura, Y. Kitagawa, Y. Miyazaki, *Chem. Lett.* **2000**, *29*, 922–923.
[17] Z. -B. Zhou, M. Takeda, M. Ue, *J. Fluorine Chem.* **2003**, *123*, 127–131.
[18] Z. -B. Zhou, M. Takeda, T. Fujii, M. Ue, *J. Electrochem. Soc.* **2005**, *152*, A351–A356.
[19] Z.-B. Zhou, M. Takeda, M. Ue, *J. Fluorine Chem.* **2004**, *125*, 471–476.
[20] a) Z.-B. Zhou, H. Matsumoto, K. Tatsumi, *Chem. Eur. J.* **2004**, *10*, 6581–6591; b) Z.-B. Zhou, H. Matsumoto, K. Tatsumi, *Chem. Lett.* **2004**, *33*, 680.
[21] a) Z.-B. Zhou, H. Matsumoto, K. Tatsumi, *Chem. Eur. J.* **2005**, *11*, 752–766; b) Z.-B. Zhou, H. Matsumoto, K. Tatsumi, *Chem. Lett.* **2004**, *33*, 886–887.
[22] Z.-B. Zhou, H. Matsumoto, K. Tatsumi, *Chem. Lett.* **2004**, *33*, 1636–1637.
[23] S. Forsyth, J. Golding, D. R. MacFarlane, M. Forsyth, *Electrochim. Acta* **2001**, *46*, 1753–1757.
[24] J. Golding, N. Hamid, D. R. MacFarlane, M. Forsyth, C. Forsyth, C. Collins, J. Huang, *Chem. Mater.* **2001**, *13*, 558–564.
[25] a) J. Kim, R. P. Singh, J. M. Shreeve, *Inorg. Chem.* **2004**, *43*, 2960–2966; b) J. Kim, J. M. Shreeve, *Org. Biomol. Chem.* **2004**, *2*, 2728–2734.
[26] K. Kim, S. Choi, D. Demberelnyamba, H. Lee, J. Oh, B. Lee, S. Mun, *Chem. Commun.* **2004**, 828–829.
[27] a) D. MacFarlane, J. Huang, M. Forsyth, *Nature* **1999**, *402*, 792–794; b) D. MacFarlane, M. Forsyth, *Adv. Mater.* **2001**, *13*, 957–966.
[28] Y. Abu-Lebdeh, P. J. Alarco, M. Armand, *Angew. Chem.* **2003**, *115*, 4637–4639; *Angew. Chem. Int. Ed.* **2003**, *42*, 4499–4501.
[29] a) J. C. Dearden, *Sci. Total Environ.* **1991**, *109/110*, 59–68; b) R. J. C. Brown, R. F. C. Brown, *J. Chem. Educ.* **2000**, *77*, 724–731.
[30] a) E. I. Cooper, C. A. Angell, *Solid State Ionics* **1983**, *9/10*, 617–622; b) E. I. Cooper, C. A. Angell, *Solid State Ionics* **1986**, *18/19*, 570–576.
[31] a) W. Xu, E. I. Cooper, C. A. Angell, *J. Phys. Chem. B* **2003**, *107*, 6170–6178; b) W. Xu, L. M. Wang, R. A. Nieman, C. A. Angell, *J. Phys. Chem. B* **2003**, *107*, 11749–11756.
[32] J. Pernak, K. Sobaszkiewicz, J. Foksowicz-Flaczyk, *Chem. Eur. J.* **2004**, *10*, 3479–3485.
[33] a) P. Bonhote, A. P. Dias, N. Papageorgiou, K. Kalyanasundaram, M. Graetzel, *Inorg. Chem.* **1996**, *35*, 1168–1178; b) J. G. Huddleston, A. E. Visser, W. M. Reichert, H. D. Willauer, G. A. Broker, R. D. Rogers, *Green Chem.* **2001**, *3*, 156–164.
[34] C. M. Forsyth, D. R. MacFarlane, J. J. Golding, J. Huang, J. Sun, M. Forsyth, *Chem. Mater.* **2002**, *14*, 2103–2108.
[35] G. Gritzner, J. Kuta, *Pure Appl. Chem.* **1984**, *56*, 461–466.
[36] A. N. Dey, *J. Electrochem. Soc.* **1971**, *118*, 1547–1549.
[37] G. A. Molander, B. P. Hoag, *Organometallics* **2003**, *22*, 3313–3315.
[38] H. Heaney, G. Papageorgiou, R. F. Wilkins, *Tetrahedron* **1997**, *53*, 14381–14396.

Received: August 1, 2005
Published online: January 3, 2006

